UNIVERSITAT POLITÈCNICA DE CATALUNYA
BARCELONATECH
Escola d'Enginyeria de Barcelona Est

FINAL MASTER THESIS

Master in Interdisciplinary and Innovative Engineering

Design and analysis of building integrated renewable energy sources onto a demo site.

Report and Annex

Author: Joseph Katmarji
Supervisor: Herminio Martinez Garcia
Department Electronic Engineering

Call: June 2023

Abstract

This Master's thesis focuses on the integration of renewable energy sources onto a specific building, 'Building I' located at the UPC, Diagonal Besòs campus in Barcelona, Spain. The objective of the study is to explore the potential of on-site energy generation and consequent CO2 emission reduction by taking advantage of the different surfaces of the building with high potential of energy generation, with an effort to decarbonize the building sector which is responsible for about 40 % of the European Union's energy consumption.

The research methodology involved creating a detailed 3D model of the building using Building Information Modelling (BIM) software Autodesk Revit and conducting solar analysis to assess the incident solar irradiation on each surface. Solar panels were strategically installed on surfaces with high solar potential based on market research and energy output calculations guided by established principles. The study also considered mini wind energy systems for roof applications but determined that solar panels provided a more efficient use of available space. The study draws its data from various sources, including web based research from research papers, industry professionals, campus directories, official regulatory and governmental bodies, and computer softwares such as Autodesk Revit, in order to make the study as accurate as possible.

The integrated renewable energy systems were found to generate a total of up to 201.853 MWh of energy annually and up to 5,691.193 MWh over a 30-year lifespan. This resulted in a reduction of approximately 1553.69 tons of CO2 emissions over the life cycle and contributed to a 38.22 % reduction in the building's energy consumption and a 6.49 % reduction in the campus' overall energy consumption. Furthermore, an economic analysis was conducted, including the calculation of the payback period and return on investment. The estimated payback period was found to be 12 years with some assumptions taken, indicating the time required to recover the initial investment through energy savings. The return on investment was determined to be 175.08 % after over a 30 year life span, demonstrating the financial viability of the integrated renewable energy systems.

Summing up, this thesis highlights the potential of building-integrated renewable energy systems to enhance energy generation, reduce CO2 emissions, and achieve significant energy consumption savings for the studied building and campus. The findings underscore the environmental and economic benefits of integrating renewable energy systems into buildings, contributing to the broader goal of sustainable energy transitions in the built environment.

Resum

Aquesta tesi de màster se centra en la integració de fonts d'energia renovables a un edifici concret, l''Edifici I', situat al campus Diagonal Besòs de la UPC, a Barcelona, Espanya. L´objectiu de l´estudi és explorar el potencial de generació d´energia in situ i la conseqüent reducció d´emissions de CO2 mitjançant l´aprofitament de les diferents superfícies de l´edifici amb alt potencial de generació d´energia, amb un esforç per descarbonitzar el sector de l´edificació que és responsable del voltant del 40% del consum energètic de la Unió Europea.

La metodologia de recerca va consistir a crear un model 3D detallat de l'edifici utilitzant el programari de modelatge d'informació d'edificis (BIM) Autodesk Revit i fer una anàlisi solar per avaluar la irradiació solar incident a cada superfície. Els panells solars es van instal·lar estratègicament en superfícies amb alt potencial solar basant-se en estudis de mercat i càlculs de producció energètica guiats per principis establerts. L'estudi també va considerar sistemes d'energia minieòlica per a aplicacions en teulades, però va determinar que els panells solars proporcionaven un ús més eficient de l'espai disponible. Perquè l'estudi sigui el més precís possible, les dades procedeixen de diverses fonts, com ara estudis a Internet de treballs de recerca, professionals del sector, directoris de campus, organismes oficials reguladors i governamentals i programes informàtics com Autodesk Revit.

Es va descobrir que els sistemes integrats d'energia renovable generaven un total de fins a 201.853 MWh d'energia a l'any i fins a 5,691.193 MWh al llarg d'una vida útil de 30 anys. Això es va traduir en una reducció d'aproximadament 1553,69 tones d'emissions de CO2 al llarg del cicle de vida i va contribuir a una reducció del 38,22% del consum energètic de l'edifici i del 6,49% del consum energètic global del campus . A més, es va fer una anàlisi econòmica que incloïa el càlcul del període d'amortització i el rendiment de la inversió. El període d'amortització estimat va ser de 12 anys amb algunes suposicions preses, cosa que indica el temps necessari per recuperar la inversió inicial a través de l'estalvi d'energia. Es va determinar que el rendiment de la inversió era del 175.08 % després d'una vida útil de 30 anys, cosa que demostra la viabilitat financera dels sistemes integrats d'energies renovables.

En resum, aquesta tesi posa de manifest el potencial dels sistemes d'energies renovables integrats a edificis per millorar la generació d'energia, reduir les emissions de CO2 i assolir un estalvi significatiu en el consum energètic de l'edifici i el campus estudiats. Els resultats subratllen els beneficis mediambientals i econòmics de la integració de sistemes d'energies renovables als edificis, contribuint a l'objectiu més ampli de les transicions energètiques sostenibles a l'entorn construït.

Resumen

Esta tesis de máster se centra en la integración de fuentes de energía renovables en un edificio concreto, el 'Edificio I', situado en el campus Diagonal Besòs de la UPC, en Barcelona, España. El objetivo del estudio es explorar el potencial de generación de energía in situ y la consiguiente reducción de emisiones de CO2 mediante el aprovechamiento de las diferentes superficies del edificio con alto potencial de generación de energía, con un esfuerzo por descarbonizar el sector de la edificación que es responsable de alrededor del 40% del consumo energético de la Unión Europea.

La metodología de investigación consistió en crear un modelo 3D detallado del edificio utilizando el software de modelado de información de edificios (BIM) Autodesk Revit y realizar un análisis solar para evaluar la irradiación solar incidente en cada superficie. Los paneles solares se instalaron estratégicamente en superficies con alto potencial solar basándose en estudios de mercado y cálculos de producción energética guiados por principios establecidos. El estudio también consideró sistemas de energía minieólica para aplicaciones en tejados, pero determinó que los paneles solares proporcionaban un uso más eficiente del espacio disponible. Para que el estudio sea lo más preciso posible, los datos proceden de diversas fuentes, como estudios en Internet de trabajos de investigación, profesionales del sector, directorios de campus, organismos oficiales reguladores y gubernamentales y programas informáticos como Autodesk Revit.

Se descubrió que los sistemas integrados de energía renovable generaban un total de hasta 201,853 MWh de energía al año y hasta 5.691,193 MWh a lo largo de una vida útil de 30 años. Esto se tradujo en una reducción de aproximadamente 1553,69 toneladas de emisiones de CO2 a lo largo del ciclo de vida y contribuyó a una reducción del 38,22 % del consumo energético del edificio y del 6,49 % del consumo energético global del campus. Además, se realizó un análisis económico que incluía el cálculo del periodo de amortización y el rendimiento de la inversión. El periodo de amortización estimado resultó ser de 12 años con algunas suposiciones tomadas, lo que indica el tiempo necesario para recuperar la inversión inicial a través del ahorro de energía. Se determinó que el rendimiento de la inversión era del 175.08 % tras una vida útil de 30 años, lo que demuestra la viabilidad financiera de los sistemas integrados de energías renovables.

En resumen, esta tesis pone de manifiesto el potencial de los sistemas de energías renovables integrados en edificios para mejorar la generación de energía, reducir las emisiones de CO2 y lograr un ahorro significativo en el consumo energético del edificio y el campus estudiados. Los resultados subrayan los beneficios medioambientales y económicos de la integración de sistemas

de energías renovables en los edificios, contribuyendo al objetivo más amplio de las transiciones energéticas sostenibles en el entorno construido.

Appreciations

I would like to express my sincere gratitude to the following individuals and organizations for their invaluable contributions and support throughout the completion of this thesis.

First and foremost, I would like to extend my deepest appreciation to my thesis advisor, Dr. Herminio Martinez Garcia, for his unwavering guidance, expertise, and continuous support. His insightful feedback has been instrumental in shaping the direction of this study. I would also like to thank faculty member Dr. Guillermo Velasco, for his valuable knowledge and the extensive literature he provided. His contributions greatly enhanced my understanding of the subject matter and served as a constant source of inspiration.

My gratitude also goes to my personal friends who assisted me with the creation of the model in the building information modeling software Revit, as using the software was a first for me and their technical expertise and willingness to lend a helping hand were invaluable in bringing the project to fruition.

Special thanks go to the university officials for providing access to the building plans and facilitated the 3D modeling, and also for the creators of the UPC Energy and Water Resources Information System (SIRENA) for its comprehensive data and insights that aim to monitor the consumption data of the university as a whole and facilitate the emergence of problem solving solutions for more sustainable campuses.

Finally, I am indebted to my own passion and curiosity that sparked my interest in the topic in the first place. This self-driven motivation has been the driving force behind the selection of the university building as a case study and the exploration of its outcomes, as I view it as a matter that alters the future of the built environment and creates more sustainable cities for a better future.

I extend my heartfelt thanks to everyone mentioned above and all others who have supported me in various ways throughout this journey. Your contributions have been crucial in the successful completion of this thesis.

Index

1. Introduction

The European Union (EU) has set ambitious targets for reducing greenhouse gas emissions to combat climate change. The EU's current target is to reduce its emissions by at least 55% by 2030 compared to 1990 levels, and achieve climate neutrality by 2050 [1]. Achieving these targets will require significant efforts in all sectors, including the built environment, which accounts for approximately 40% of the EU's total energy consumption and 36% of its greenhouse gas emissions [2]. As such, reducing the carbon footprint of buildings is critical to mitigate the matter of climate change and pave the way for a greener future.

To achieve these ambitious targets, the EU has put in place various policies, initiatives and legislation aimed at promoting sustainable development in the built environment. One of these policies is the Energy Performance of Buildings Directive (EPBD), which sets out minimum energy performance standards for buildings in the EU and requires member states to establish long-term renovation strategies to improve the energy efficiency of their buildings [3]. In addition, the city of Barcelona has demonstrated its unwavering commitment to promoting sustainable development in the built environment through the implementation of a wide array of innovative initiatives and progressive policies. These efforts have been instrumental in fostering the adoption of renewable energy sources and driving the integration of energy-efficient technologies, paving the way for a greener and more environmentally conscious cityscape.[4]

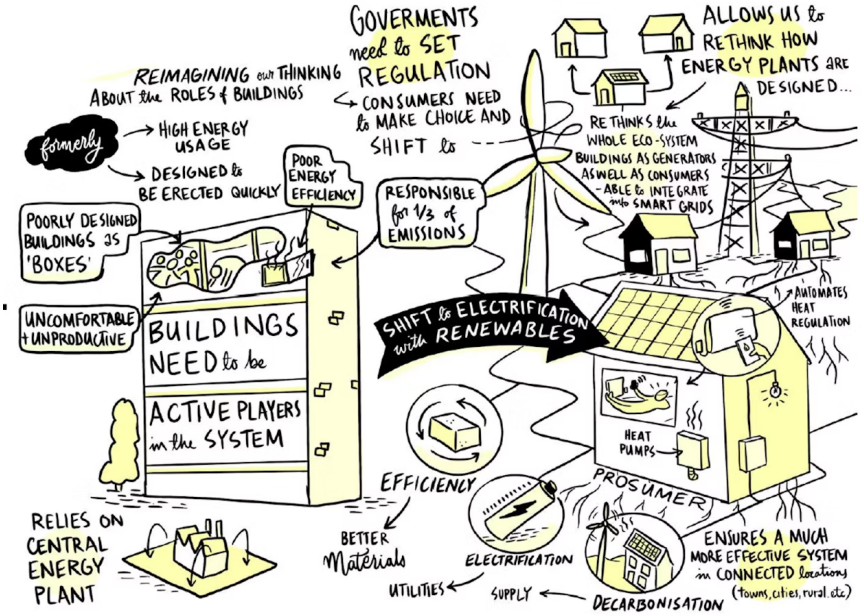

Figure 1.1. The state of buildings and future perspectives. [32]

Building-integrated renewable energy systems (BIRES) have emerged as a promising strategy for reducing energy consumption and emissions [5]. By integrating renewable energy sources such as solar photovoltaic (PV) panels and wind turbines onto the building envelope (Roofs, curtain walls, awnings,windows, etc.) to generate electricity, clean energy can be produced and therefore, reduce the reliance on fossil fuels while also providing multiple benefits such as improved indoor comfort, reduced energy costs, and perhaps enhanced architectural aesthetics [6].

This master's thesis aims to contribute to these efforts by designing and examining the outcomes of integrating renewable sources into a demonstration building, referred to as Building "I", located at the EEBE campus of Universitat Politècnica de Catalunya, and investigate the potential energy offset and carbon emission reduction achievable through the implementation of these systems.

In this outline, we will present the methodology and the design considerations for developing these systems. The study will start with a state of the art on the existing renewable energy technology as well as the electronic components that complement it, in addition to incentives and all the relevant information that make this study viable and worthy. A detailed design will be proposed, and simulations will be conducted and finally, the study's conclusion will discuss the potential of BIRE systems in contributing to the green goals, the challenges that might be encountered and the possibility of wider adoption of similar solutions in the built environment.

2. State of the Art

2.1. Solar Systems

Solar technology is a rapidly growing field that involves the conversion of sunlight into usable energy. It has the potential to be a significant source of renewable energy, and there have been many technological advancements in recent years that have made it more efficient and cost-effective. One of the most commonly used solar technologies is photovoltaic (PV) technology, which involves the use of solar cells to convert sunlight into electricity. These cells are made of semiconductor materials, and when exposed to sunlight, they generate a flow of electricity[7]. One of the main advantages of solar technology is its scalability. Solar panels can be installed on residential or commercial buildings to generate electricity for the building's occupants. Alternatively, large-scale solar farms can be developed to provide electricity to entire communities. As a result, solar technology can be adapted to meet a wide range of energy needs [8].

Advancements in solar technology have led to increased efficiency and reduced costs as per the data presented in figures 2.1 and 2.2. The efficiency of solar cells has improved significantly in recent years, with some cells reaching efficiencies of up to 40% [9]. In addition, the cost of solar panels has decreased by more than 80% over the past decade, making solar technology more competitive with traditional energy sources [10]. There are also ongoing developments in the materials used for solar cells. For example, perovskite solar cells have shown promise due to their high efficiency and low production costs. However, their stability and durability remain a challenge for commercial use [11].

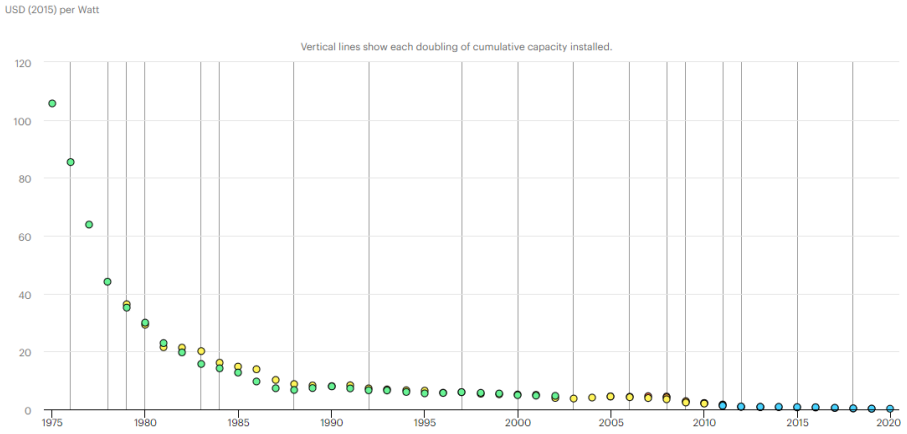

Figure 2.1. The decrease of the Price per Watt for solar modules (1975-2020) [12]

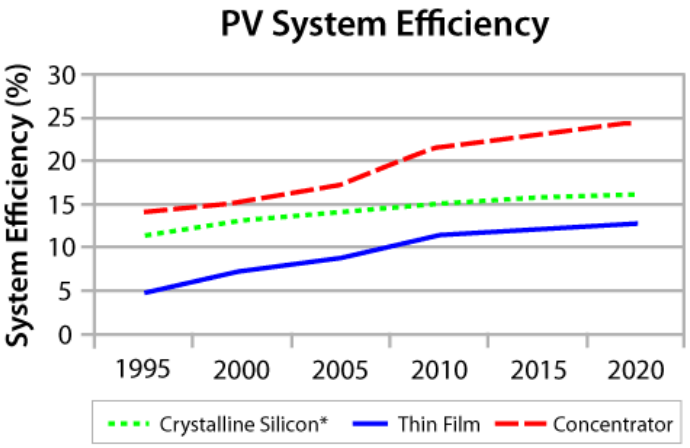

Figure 2.2. The increase of efficiency of solar modules (1995-2020) [13]

Overall, solar technology has the potential to play a significant role in meeting the world's energy needs. With ongoing advancements in the horizon and decreasing costs, it is becoming an increasingly viable alternative to traditional energy sources.

Some of the most commonly used types of solar cells:

2.1.1 Monocrystalline Cells

Monocrystalline solar cells are a type of photovoltaic cells that are manufactured from a single crystal of silicon, making them one of the oldest and most efficient solar cell technologies available [14]. The cells are produced by slicing a cylindrical ingot of pure silicon into thin wafers, which are then doped with impurities to create p-type and n-type silicon layers. The process results in a highly pure and uniform material, which allows the cell to have a high level of efficiency and durability. Monocrystalline cells typically have an efficiency range of 17-22%, which is higher than other types of solar cells such as polycrystalline or thin-film cells. Researchers have also explored the use of new materials and fabrication techniques to increase cell efficiency, such as incorporating carbon nanotubes into the cells or developing textured silicon surfaces to trap more light [15].

Monocrystalline cells offer several advantages over other solar cell types. They are highly efficient, making them an attractive option for residential and commercial applications. They are also highly durable and have a longer lifespan compared to other types of cells, as they are less susceptible to

cracking or degradation over time. However, they are more expensive to manufacture than other types of cells, and their efficiency can be affected by shading or high temperatures [16].

2.1.2. Polycrystalline Cells

Polycrystalline solar cells are another type of photovoltaic cells that are made from multiple silicon crystals, making them cheaper to produce than monocrystalline cells [17]. The cells are created by melting and casting silicone into ingots, which are then cut into thin wafers. Polycrystalline cells have a characteristic blue hue due to the random orientation of the crystals on their surface.

Polycrystalline cells have lower efficiencies than monocrystalline cells, typically ranging from 15-17% [17]. However, their lower production costs make them an attractive option for large-scale commercial applications. They are also less sensitive to high temperatures and shading than monocrystalline cells. Researchers have explored various approaches to increase cell efficiency, such as incorporating nanostructures into the cell's surface to trap more light or developing new materials to replace silicon, such as copper indium gallium selenide (CIGS) or perovskite materials [18].

2.1.3. Thin-film Cells

Thin-film solar cells are a relatively newer technology that uses thin layers of semiconductor materials to convert sunlight into electricity. Unlike crystalline silicon cells, thin-film cells are made by depositing a thin layer of semiconductor material on a substrate. This allows for flexibility in the manufacturing process and makes the cells lightweight and easy to install. However, thin-film cells have lower efficiencies (7 to 13%) than crystalline silicon cells and can degrade over time [19].

One type of thin-film technology is cadmium telluride (CdTe) solar cells, which has a relatively low manufacturing cost and high efficiency in converting sunlight into electricity. Another type is copper indium gallium selenide (CIGS) solar cells, which has the highest efficiency among thin-film technologies but is more expensive to manufacture. Other thin-film technologies include amorphous silicon (a-Si) and organic photovoltaic (OPV) cells [20].

Despite their lower efficiencies, thin-film cells have advantages in certain applications, such as in building-integrated photovoltaics (BIPV) and portable solar devices. Ongoing research and development in thin-film technology aim to increase their efficiency and decrease manufacturing costs, making them a more viable option for larger-scale solar installations [21].

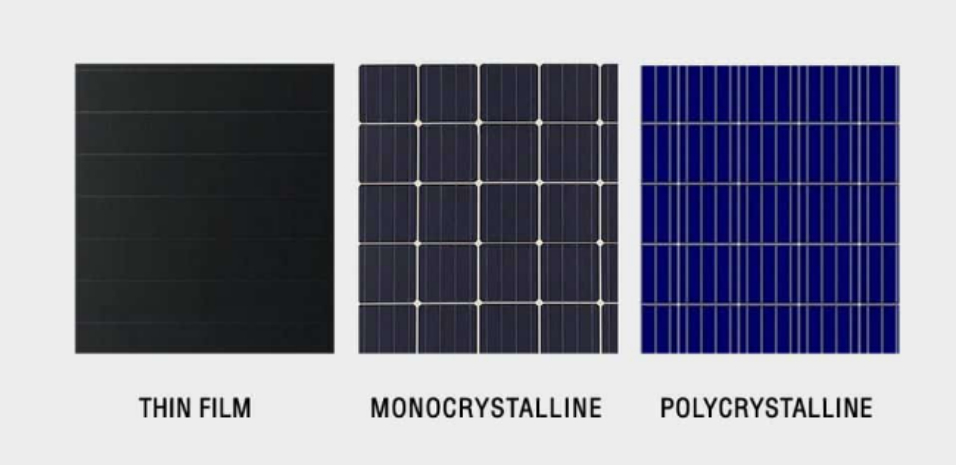

Figure 2.3.A visual comparison between the different types of solar cells

2.2. Micro Wind Systems

Micro wind turbines are small-scale wind turbines typically used to generate electricity for homes, farms, and small businesses. These turbines have evolved over time to become more efficient, quieter, and less expensive. The earliest versions of mini wind turbines were mainly used in remote locations without access to a power grid and they were often noisy, inefficient, and expensive, which limited their use. However, with advancements in technology, mini wind turbines have become more practical and cost-effective. [22]

One major development in mini wind turbine technology has been the use of lighter and stronger materials for the blades. Early turbines used wooden or fiberglass blades, which were heavy and susceptible to damage. Modern turbines now use lightweight materials like carbon fiber or aluminum, that can withstand harsh weather conditions. [23]

In recent years, there has been an increasing interest in vertical axis wind turbines (VAWTs) as an alternative to traditional horizontal axis wind turbines (HAWTs). VAWTs have the advantage of being able to operate in turbulent wind conditions and are less sensitive to wind direction. However, they are generally less efficient than HAWTs and are still relatively new in the market. [24].

Overall, micro wind turbines have come a long way since their inception, and with continued advancements in technology, they have the potential to become an increasingly important source of renewable energy.

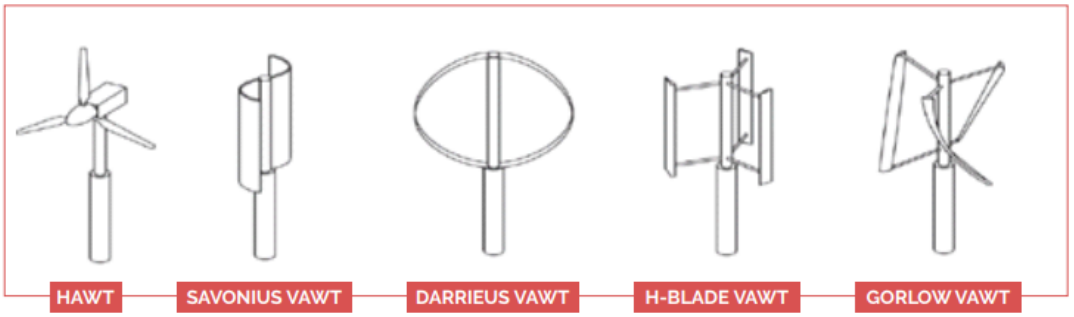

Figure 2.4 Different types of wind turbines.

2.3 Inverters

Inverters are a crucial component in renewable energy systems, responsible for converting the direct current (DC) electricity produced by the systems into alternating current (AC) electricity that can be used in homes or businesses. In recent years, there have been significant advancements in inverter technology, aimed at improving their efficiency, reliability, and cost-effectiveness.

One important advancement in inverter technology is the use of transformerless inverters. These inverters use capacitors to reduce the size and weight of the inverter, making them more compact and easier to install. They also have higher efficiency and lower standby power consumption compared to traditional inverters with transformers [25]. Another important development in inverter technology is the integration of maximum power point tracking (MPPT) algorithms. MPPT algorithms allow inverters to optimize the power output of solar panels by continuously tracking the maximum power point of the panels. This results in higher energy yield and improved system efficiency [26].

Inverters are also becoming smarter and more connected. Smart inverters can communicate with other components of a solar PV system and with the grid, allowing for better monitoring and control of energy flow. This is important for managing the intermittency of renewable energy sources and for maintaining grid stability [27].

There has also been a trend towards the use of hybrid inverters, which can manage both solar PV and battery storage systems. These inverters allow for greater flexibility in energy management, allowing excess energy to be stored in batteries for later use. Hybrid inverters can also provide backup power in case of grid outages [28].

There are three main types of inverters for solar systems :

1-String inverters: the most common type of inverter used in PV systems. They are a central unit that is connected to all the solar panels in the system. The panels are connected in series to create a string, and the inverter converts the DC electricity produced by the string to AC electricity that can be used in homes or businesses. However, string inverters have some disadvantages, including potential shading issues and reduced efficiency due to voltage drops [29].

2-Microinverters, on the other hand, are installed on each solar panel and convert the DC electricity generated by each panel to AC electricity. This design allows each panel to operate independently, eliminating shading issues and maximizing system efficiency. Microinverters also offer increased safety, as the DC voltage is reduced to a safer level [29].

3-Power optimizers are a hybrid of string inverters and microinverters. They are installed at the module level, like microinverters, but they still use a central inverter to convert the DC electricity to AC electricity. Power optimizers offer the benefits of microinverters, including independent operation and improved system efficiency, while still allowing for the use of a central inverter [29].

As for wind systems, one type of inverter commonly used in wind energy systems is the grid-tie inverter. This type of inverter is designed to synchronize the output of the wind turbine with the electrical grid. Grid-tie inverters are generally small and lightweight, making them ideal for residential and small-scale wind energy systems. The continuous improvement of inverters is essential for the growth of renewable energy and contributes towards achieving more efficient, reliable, and cost-effective renewable energy systems.

2.4 Grid Connected Systems

Grid-connected renewable energy systems have become increasingly popular as a way to generate clean energy while still being connected to the utility grid. These systems are designed to generate electricity using renewable sources and then feed any excess power back into the grid. In this way,the grid serves as a "virtual battery" to store the excess energy and distribute it to other consumers when needed [30]. These systems are typically connected to the utility grid through an inverter and excess electricity generated by the system is sent back to the grid, and the homeowner or business owner receives a credit on their electricity bill for the energy they have generated. [31]

In addition to grid-tied systems, there are also off-grid renewable energy systems that are not connected to the utility grid. These systems typically include a battery bank to store excess energy generated by the system, which can then be used when the renewable energy source is not available. Off-grid systems are typically more expensive to install than grid-tied systems, but they can be a good option for homes or businesses in remote areas that are not connected to the grid. [30]

Grid-connected renewable energy systems are a promising solution to our current energy challenges. As technology continues to improve and costs continue to drop, we can expect to see more and more homes and businesses adopting these systems as a way to reduce their carbon footprint and save on energy costs [31].

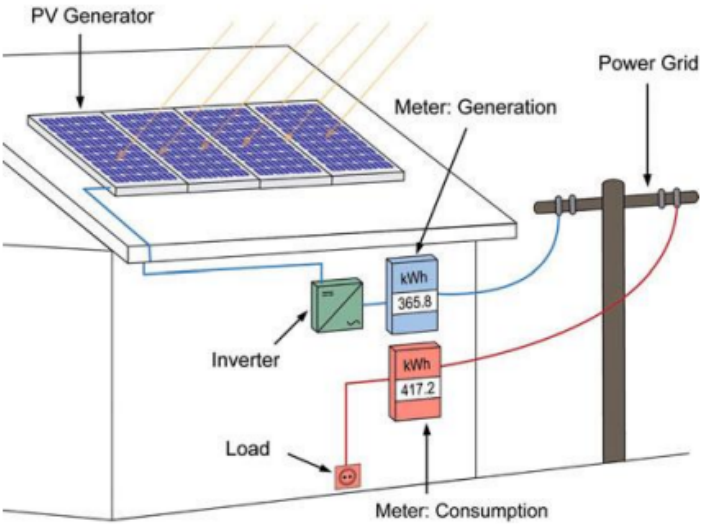

Figure 2.5 A schematic on Grid connected systems.[31]

2.5 Net/Near Zero Energy Buildings

Buildings currently consume a significant portion of the world's energy, making them a critical component in achieving net-zero emissions. As such, buildings must transition from passive and inefficient energy consumers into active participants in the energy system by integrating renewable energy sources and adopting energy efficiency measures. This transformation would allow buildings to interact with the energy grid and reduce demand spikes, leading to lower electricity costs and increased control over energy use for consumers. Additionally, the integration of renewable energy sources would help to ease congestion in the grid and reduce greenhouse-gas emissions associated with fossil fuels. [32]

In the coming decade, buildings will play an increasingly important role in the energy system by providing flexibility to the system. This will allow for efficient integration of variable solar and wind power by using electricity generated by these sources for building purposes.[33]

2.5.1. BIPV / BAPV

Building-attached photovoltaics (BAPV) are photovoltaic modules that are mounted on a building envelope without fulfilling the following criteria for building integration: mechanical rigidity or structural integrity, primary weather impact protection such as rain, snow, wind, and hail, energy economy considerations such as shading, daylighting, and thermal insulation, fire protection, noise protection, separation between indoor and outdoor environments, and security, shelter, or safety measures.[34]

Building-integrated photovoltaics (BIPV) refers to the incorporation of photovoltaic modules into a building's construction in a way that serves a function for any of the criteria previously mentioned in addition to generating energy, and if they need to be removed, an appropriate replacement construction product is necessary.[34]

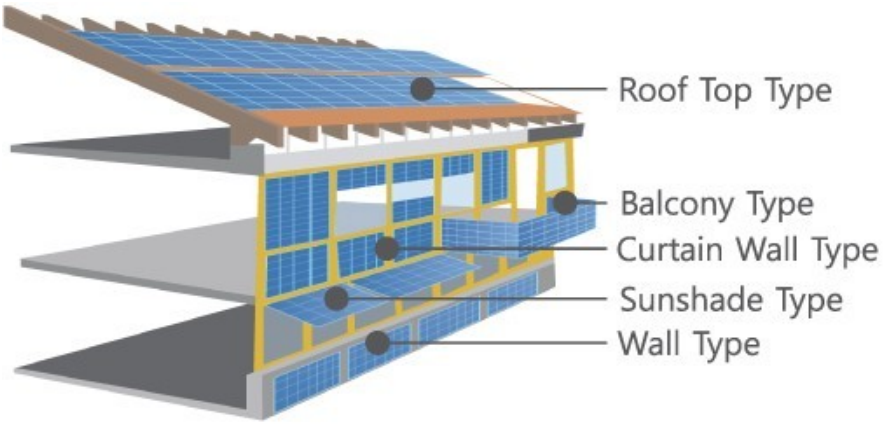

Figure 2.6 Examples of BIPV elements [35]

BIPV products are emerging into the markets worldwide and various types of products are being developed for suitable architectural integration, however, compared to traditional solar modules, BIPVs have lower efficiencies and higher costs due to manufacturing complexities, architectural integrity and aesthetics.

Some examples of BIPV Products available in the market (Source: SolarInnova Manufacturers) :

Awnings

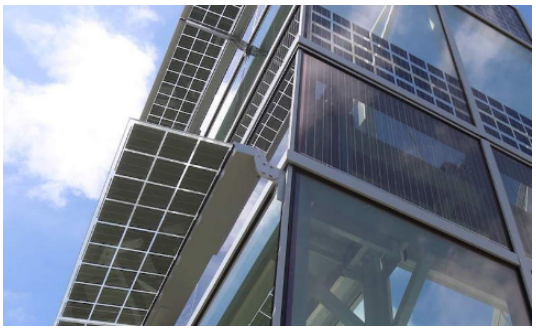

Figure 2.7 BIPV Awnings

Balcony Railings

Figure 2.8 BIPV Balcony Railings

Curtain Walls

Figure 2.9 BIPV Curtain walls

2.5.2. BIWT

Initially, small wind turbines were designed with a horizontal axis (HAWTs). However, due to their need for a high tower and unappealing aesthetics, vertical axis wind turbines (VAWTs) became more popular, especially for integrated building applications. In addition, VAWTs operate more quietly than HAWTs, reducing noise disturbance. With rated power ranging from 200W to 10kW, VAWTs can function as standalone or grid-connected systems and can be combined with other energy conversion technologies, like photovoltaics. Small wind turbines, with heights between 2 to 10 meters, can be installed on rooftops, streets, or gardens with minimal visual impact and can generate energy from moderate wind speeds. [36]

Figure 2.10 Wind System building integration options: (a) Large systems (b) Micro Systems [37]

Micro wind turbines are commonly set up in places that experience strong and frequent winds. Before installing a wind turbine, it's crucial to gather wind data in the surrounding area of the building or site. Using this wind data, a suitable type of wind turbine can be chosen, and the ideal location can be identified to optimize electricity production. A critical factor is to align the wind conditions of the location with the wind turbine's cut-in, rated, and cut-out wind speeds. [36]

Solar-wind hybrid systems are a combination of two renewable energy technologies that have been rapidly growing in popularity. This idea has arisen from the fact that solar and wind power are complementary. Solar power relies on sunlight and can only generate energy during daylight hours, typically from 8 am to 6 pm. Wind power, however, starts picking up in the late evening and

reaches its maximum output during the night. By combining wind and solar power, the variability in power production can be smoothed out over the course of the day.[36]

2.6. Barcelona: Initiatives and Incentives

Barcelona has a history of taking action to combat climate change, having implemented various plans since 2002. These plans are designed to reduce the city's greenhouse gas emissions, increase the use of renewable and locally-sourced energy, improve energy efficiency, and prepare for anticipated impacts. The city is dedicated to achieving energy sovereignty by reducing energy consumption through responsible usage and efficiency, self-sufficiency, and by generating as much renewable energy as possible using locally-sourced resources, while also ensuring that all citizens have access to a basic energy supply. [38]

For this reason, the City Council promotes the use of rooftops and public spaces for solar energy production. They offer assistance through subsidies and tax advantages as part of their strategy to boost solar energy generation. In 2019 and 2020, the Council provided subsidies of up to 50% of the cost of voluntary installations of photovoltaic panels for electricity production. Additionally, the Council supports energy consumption reduction in buildings by subsidizing up to 40% of the cost of comprehensive energy improvement measures (such as insulation throughout the building envelope) or up to 25% of the cost of partial energy rehabilitation measures (including facades, roofs, partition walls, and vaults).[39]

Residential buildings are among the primary energy users in Barcelona, but there is an opportunity to transform these homes into small-scale power plants that generate clean energy and offset their consumption. Thanks to the city's favorable climate, which provides ample sunshine, and the increasing efficiency and accessibility of renewable energy technologies, this transformation is already possible, and the generation is encouraged using photovoltaic solar energy, solar thermal energy and mini-wind turbines. [40]

3. Methodology

3.1. Demo site assessment

3.1.1. Geographical and meteorological data

The selected demo site was Building 'I', located on the new Diagonal-Besòs Campus (EEBE) of the Universitat Politècnica de Catalunya (UPC). This building comprises 8 floors and a 13,202 m2 total area and hosts research groups in Materials Engineering and Chemical Engineering.

The building coordinates are 41° 24 '51.4"N,2° 13' 25.7"E, located on the coast of Barcelona in the northern hemisphere where a mediterranean climate is present and moderate to high levels of solar irradiance is received.

Figure 3.1 Top view of the Campus and Building "I" (in red). (Source: Google Maps)

According to the energy generation potential map provided by the Barcelona City Council (Figures 3.2 and 3.3) [41] , the demo site happens to be just outside the covered region, it can be assumed that its properties are the same as the other buildings on the same coastal line, which in this case, according to the given legend, for photovoltaic applications the potential is very good ('molt bo' in Catalan) in the area in question however, for wind systems the potential is low ('baix' in Catalan) which may be suitable for mini wind turbine applications that do not require high wind speeds.

Figure 3.2 Photovoltaic potential map (Barcelona). [41]

Figure 3.3 Wind potential map (Barcelona). [41]

3.1.2. Campus and Building Energy demand

In the demo site assessment, the energy demand of building "I" was assumed to fall in a range of 15% to 20% of the whole campus consumption. In this study, the building consumption was assumed to be 17% taking into account its relative size and activity compared to other buildings on the campus.

To put the energy demand of building "I" into perspective, the overall yearly consumption of the entire campus was determined to be 3,346,941.00 kWh. This figure represents the total energy consumed by all the buildings and facilities within the campus over the course of a year. Understanding the scale of the campus's energy consumption is crucial for evaluating the potential impact of integrating renewable energy systems and assessing the effectiveness of energy offset and carbon emission reduction strategies.

In figure 3.4 below is a visual representation of the energy consumption patterns, a graph was generated from the SIRENA platform illustrating the monthly consumption trends over the past year up until the present day, From May 2022 until may 2023.

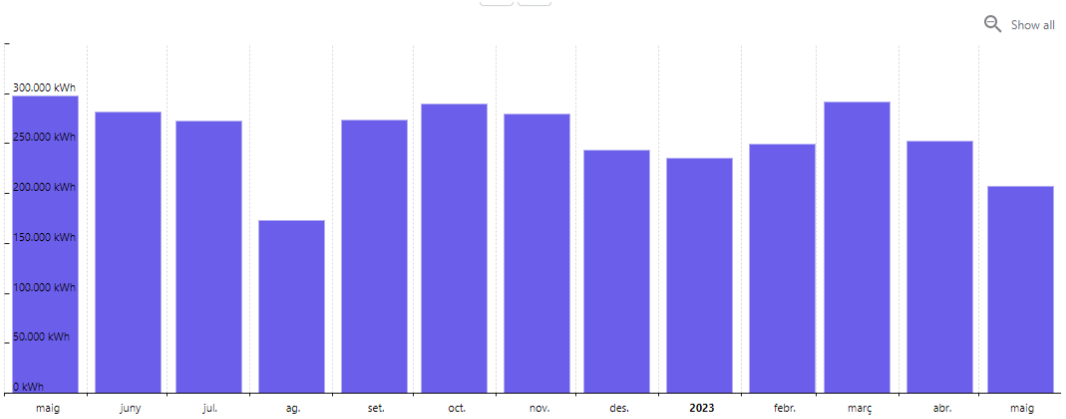

Figure 3.4 Monthly consumption in kWh of Diagonal-Besòs Campus. [44]

3.2. Design Considerations and Criteria

For simplicity, each of the building's surfaces is labeled for ease of referral as shown in Figure 3.5 below, and it consists of 7 different surfaces:

1- High Roof
2- Terrasse
3- Facade 1-A (Orientation: Southwest)
4- Facade 1-B (Orientation: Southwest)
5- Facade 2 (Orientation: Southeast)
6- Facade 3 (Orientation: Northeast)
7- Facade 4 (Orientation: Northwest)

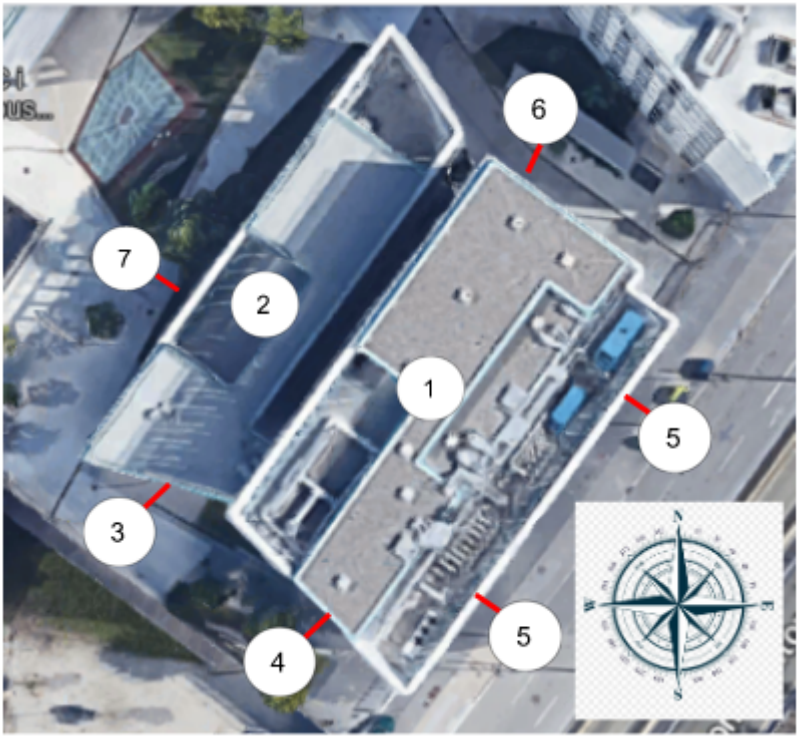

Figure 3.5 Area Labeling with building orientation.

As the building is located in the northern hemisphere, the highest solar potential must be on all south facing areas which are areas 3, 4, and 5 and in the case of building "I", these surfaces are completely exposed with no shading interference on them.

There are multiple criteria that require careful consideration for an adequate design of PV and wind systems. For the PV system design, a study on the solar irradiation that our demo site is subjected to on each of the roof and facades is required to maximize the potential, as well as the area available for module installation on each of the surfaces. As for wind systems, wind speed and direction are essential for the design at the specific location and should be carefully considered for increased performance.

3.2.1. Wind Systems Criteria

The first step in designing a wind system is to assess the wind resource at the project site. According to VortexFDC [43], which is an interface that provides valuable insights into wind direction and other factors that impact the design and performance of a wind system, the dominant wind direction is found to be from West-North-West, as shown in figure 3.6 below, which means that the wind system placement should be selected accordingly with minimal wind obstructions coming from that direction.

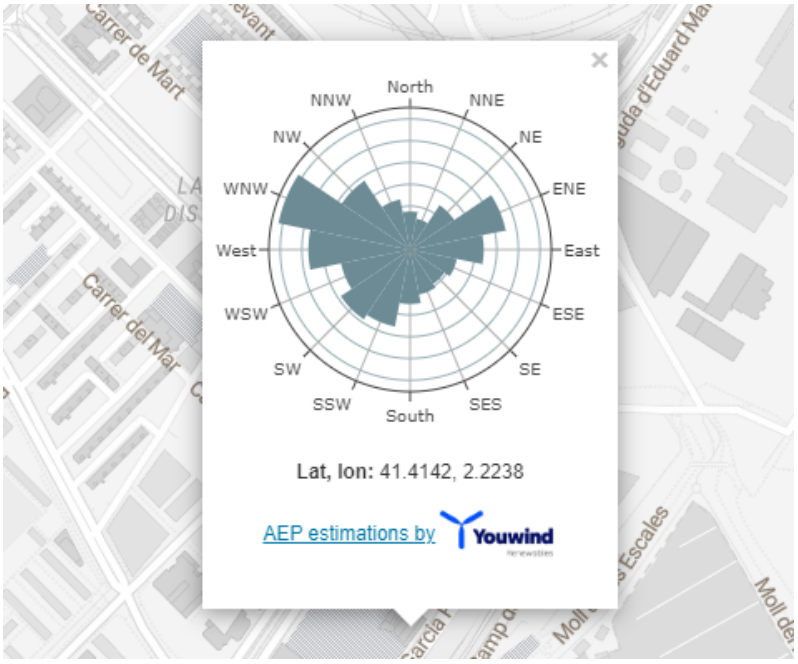

Figure 3.6 Wind Rose at demo site location. (Source: VortexFDC) [43]

As for the wind speed, using the CENER (Centro nacional de energías renovables) wind tool "Iberian Wind Map" [42], the weibull distribution of the wind speed at a 50 meters hub height at the exact site location was obtained and shown in figure 3.7 below, this data will enable the estimation of annual potential energy production of a wind system based on wind speed frequencies and the wind system's technical specifications.

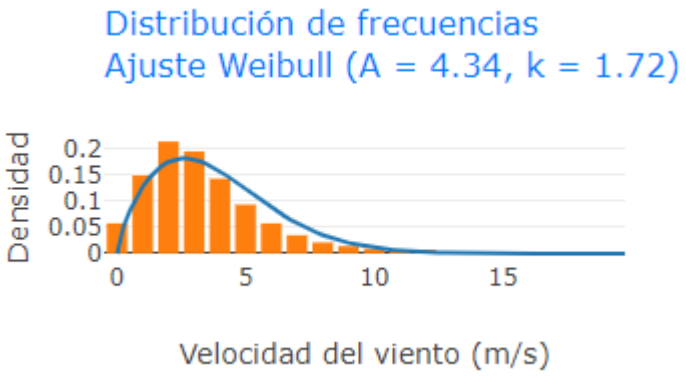

Figure 3.7 Weibull Distribution at 50m at site location. [42]

Additionally, when multiple wind turbines are to be placed in one area, an adequate separation between them is recommended, as per Figure 3.8, to minimize the wake effect of one wind turbine on others, as follows:

7 to 10 rotor diameters in the dominant wind direction and 3 to 5 rotor diameters perpendicular to dominant direction.

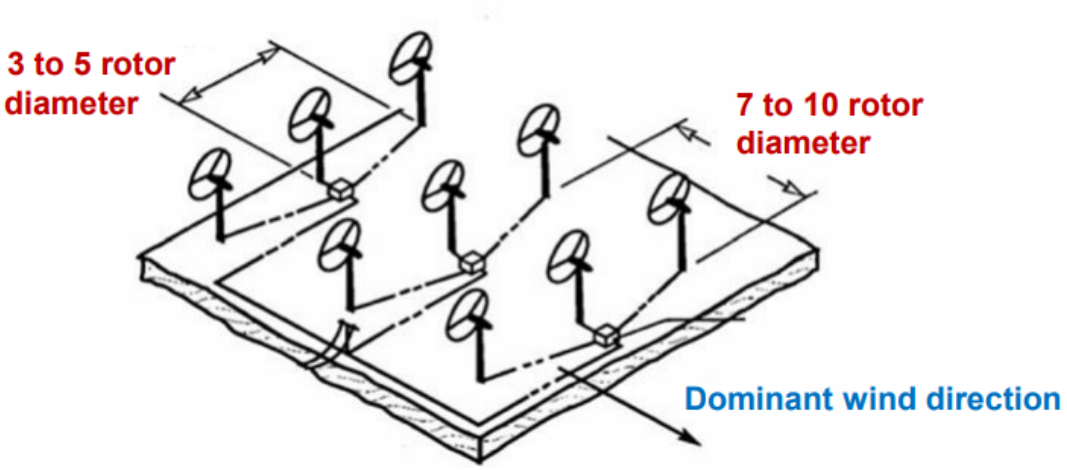

Figure 3.8 Adequate wind turbine separation.

3.2.2. Solar PV Systems Criteria:

For solar systems, it is critical to know the amount of solar irradiation that a surface is exposed to, in order to calculate the potential energy output of this surface when a solar module is placed on it. The BIM (Building Information Modelling) software Revit, which is a powerful platform widely used by architects, engineers, and construction professionals to design and simulate buildings and structures. Insight is an add-on to the software that provides solar radiation analysis for a building at a specific location, showing the amount of solar radiation on each of the building's surfaces and visualizing the sun path diagram.

For this purpose, with the help of university officials who provided the building plans and some measurements that had to be taken on site, an exact 3D model of the demo site "Building I" was created using Revit and with the exact location of the site and building orientation, a monthly solar radiation analysis using the insight add-on was obtained in kWh/m^2 in order to estimate the potential energy production for each of the facades and roof and identify the surfaces with the most potential for installing solar modules, as can be seen in the figures 3.9 and 3.10 below, where different surfaces are coloured according to the their corresponding level of solar incidence. The figures 3.9 and 3.10 show the solar analysis on all the buildings at once, but the data extraction was done on each surface individually for more accurate values in a smaller range.

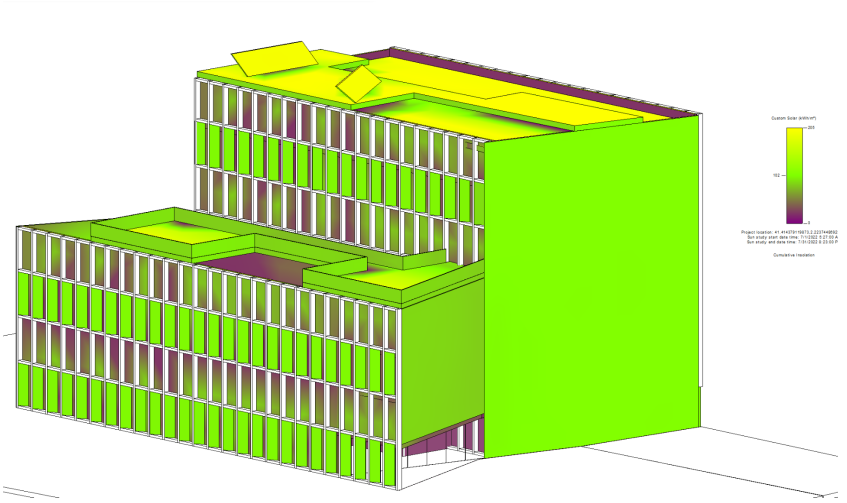

Figure 3.9 Solar Irradiation Measurements (Areas 1,2,3,4 and 7).

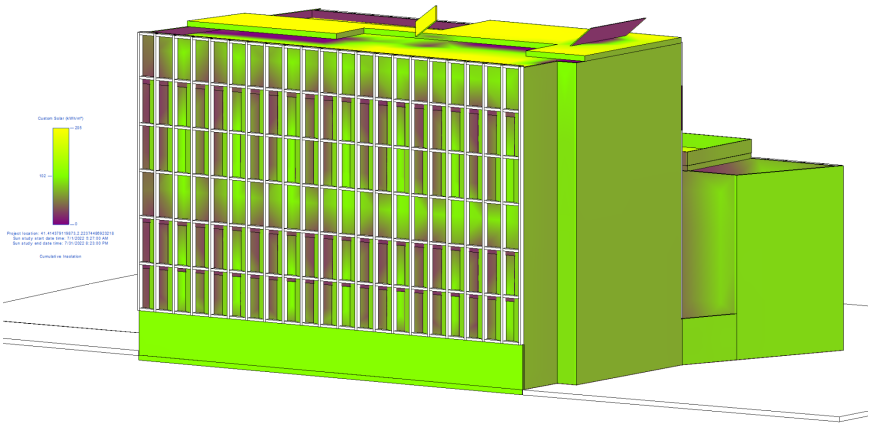

Figure 3.10 Solar Irradiation Measurements (Areas 5 and 6).

Additionally, the amount of solar radiation received on a solar module plane varies greatly with different tilt and orientation configurations. In some of the areas, the tilt and orientation configuration is restricted to the surface, while in other areas, they are configurable, and therefore, different plane configurations were designed on the surfaces using the CAD software and were oriented towards the south as much as physically possible to maximize radiation capture and increase energy production.

For tilted configurations, modules in rows might cast shade onto the ones on the row behind. Which is why row distancing should be taken into account in order to avoid losses from shadowing. The minimal distance between rows is calculated using equation 3.1 below:

$$D_{min} = \frac{L.\,sin(\beta)}{tan(61^{o} - \Phi)} + L.\,cos(\beta) \qquad \textbf{(Eq. 3.1)}$$

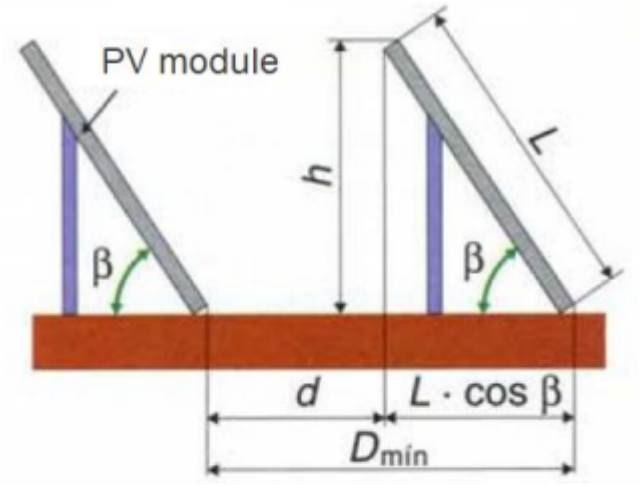

Figure 3.11 Tilted panels distancing.

Where

- $\mathbf{D_{min}}$ is the minimum row distance to prevent shading in meters (m).

-L is the length of the PV module in meters (m).

- is the tilt angle in Degrees.

-ϕ is the latitude of the considered location in Degrees.

Another important criteria for solar systems is the monthly average ambient temperature. The performance of solar cells and modules is influenced by ambient temperatures, and understanding this effect is crucial for accurate system design and performance estimation. As temperature increases, the electrical output of solar cells tends to decrease. This is primarily due to the temperature dependence of the semiconductor material used in the cells, which typically exhibits a negative temperature coefficient. This data was obtained and presented in figure 3.12 and was taken into account into the performance and energy yield of the selected solar modules.

	January	February	March	April	May	June	July	August	September	October	November	December
Avg. Temperature °C (°F)	7.9 °C (46.2) °F	8.5 °C (47.3) °F	10.9 °C (51.7) °F	13.5 °C (56.2) °F	17 °C (62.6) °F	21.3 °C (70.4) °F	23.8 °C (74.9) °F	23.9 °C (75) °F	20.9 °C (69.5) °F	17.4 °C (63.4) °F	12.1 °C (53.8) °F	8.6 °C (47.6) °F

Figure 3.12 Monthly ambient temperatures in Barcelona. [45]

3.3. Product Selection criteria and calculation methods

3.3.1. Wind Systems

For wind systems, as they can only be placed on the roof, efficiency and high power output are required, combined with good architectural integration that harmonizes with the spatial constraints of the roof and also ensures minimal noise and vibration impact through the whole array. The model's power curve, rotor diameter, and hub height are taken into account for integration suitability. Cut-in and cut-out speeds are to be also considered with respect to the wind frequencies of the area.

After the model selection, based on the wind potential of the area, the annual energy output is estimated using the model technical sheet, which includes information about the net annual energy output with respect to the average annual wind speed. The weibull distribution of the wind speed at a h= 50 meters hub height is corrected to the height where the turbine will be installed. Equations 3.2, 3.3 and 3.4 are used to calculate the new Weibull parameters 'A' the scale parameter in m/s and 'k' the shape parameter at the installation height, in this case, at approximately h'= 26 m.

$$k' = k \,.\, \left(\frac{1-0.088.\, ln\,(\frac{h}{10})}{1-0.088.\, ln\,(\frac{h'}{10})}\right) \qquad \textbf{(Eq. 3.2)}$$

$$A' = A \,.\, \left(\frac{h'}{h}\right)^{\beta} \qquad \textbf{(Eq. 3.3)}$$

$$\beta = \frac{0.37-0.088.\, ln\,(A)}{1-0.088.\, ln\,(\frac{h}{10})} \qquad \textbf{(Eq. 3.4)}$$

Having obtained the new weibull distribution parameters at installation height, the energy output will then be determined from the power curve provided by the manufacturer or the annual energy output based on the annual average wind speed.

3.3.2. Solar PV Systems

For solar systems, the panels were selected based on their efficiency and the total potential array output with respect to their dimensions. Different solar modules were considered for every area and the panel array with the highest energy output given the area constraints was chosen. High quality products are needed for safety and long term reliable operation, with minimal annual degradation and adequate temperature coefficients.

The dimensions of the available area for each of the 7 surfaces were obtained from on-site taken

measurements and some from google maps measurements. With an extra margin taken into consideration for errors, the possible number of rows and number of modules per row for each particular model are obtained for each area, then the energy output is calculated using equation 3.5 below.

$$E_M = \frac{H_M}{G_{STC}} \cdot P_{P,PVG} \cdot FL_S \cdot PR \qquad \textbf{(Eq. 3.5)}$$

Where

- $\mathbf{E_M}$ is the monthly energy delivered to the grid. (kWh)

-H_M is the monthly value of the irradiation received on the PV generator plane. (kWh/ m^2)

-G_{STC} is the irradiance in Standard Test Conditions (STC) (1000 W/m^2)

-P_{PVG} is the PV generator Peak Power (W_p or kW_P)

-FL_S is the shading loss factor. (in terms of per unit)

-PR is the performance ratio which is an index for evaluating the efficiency of a PV system under operational conditions. (in terms of per unit)

The monthly value of the irradiation received on the PV generator plane $\mathbf{H_M}$ is obtained from the Revit software on each of the surfaces in question, the shading loss factor $\mathbf{FL_S}$ is assumed to be 1. This factor is used to account for the potential reduction in solar energy generation caused by shading on the solar modules. Given the limited shading conditions on the building's useful surfaces and its favorable exposure to sunlight, it is anticipated that the shading impact is minimal.

The PV generator Peak Power $\mathbf{P_{PVG}}$ represents the number of panels that can fit in one area multiplied by the peak power of each panel. The peak power of every panel was calculated for each month taking into account the effect of ambient temperature on the cell temperature, which alters the power output based on the module's temperature power coefficient provided by the manufacturer in % / ^oC.

The power losses that occur due to temperature are calculated using equation 3.6 below:

$$P\,(at\ T_{cell}\ ^{o}C\,) \;=\; P\,(at\ 25\ ^{o}C\,)\,.\,(1 + k_{T}\,.\,(T_{cell} - 25)) \qquad \textbf{(Eq. 3.6)}$$

Where

- **P** is the rated peak power of the solar module (W_p)

-k_T is the power temperature coefficient provided by the module manufacturer (% / ^{o}C)

-T_{Cell} is the cell temperature (^{o}C)

As the cell temperature depends on the ambient temperature and the mounting of modules, cell temperature was estimated using equation 3.7 below :

$$T_{cell} \;=\; T_{ambient} + \kappa\,.\,G \qquad \textbf{(Eq. 3.7)}$$

Where

-**T_{Cell}** is the cell temperature (K)

-**$T_{ambient}$** is the ambient temperature (K)

-κ is the Ross coefficient. (K.m^2 / W)

-G is the irradiance on the module's plane (W/ m^2)

The value of the ross coefficient κ depends on the level of integration of the module and the size of air gap behind the modules. It usually ranges between 0.02 and 0.04 K.m^2 / W, Table 3.1 lists different values for different mounting conditions.

PV array type	k (Km^2/W)
Well cooled	0.02
Free standing	0.0208
Flat on roof	0.026
Not so well cooled	0.0342
Transparent PV	0.0455
Façade integrated	0.0538
On sloped roof	0.0563

Table 3.1 Ross coefficients for different mounting configurations. [47]

The irradiance on the module's plane **'G'** expressed in W/m^2 is calculated based on the irradiation data obtained from Revit following Equation 3.8:

$$G = \frac{H_M}{hs} \qquad \textbf{(Eq. 3.8)}$$

Where

- $\mathbf{H_M}$ is the monthly value of the irradiation received on the PV generator plane. (kWh/m^2). (Source:Revit)

-**hs** is the number of sun hours in the month.

The last factor of equation 3.5, the performance ratio **PR** provides an indication of how effectively the PV system is converting solar energy into usable electricity.It takes into account various factors that can affect the system's performance, which include PV modules mismatch losses, Soiling losses , disorientation losses, spectral and angular losses, temperature losses, AC and DC wiring losses, inverter losses.

PV modules mismatch losses are losses caused by slight differences in the electrical characteristics of the PV modules that form a PV generator. In this study,all the modules in every PV generator designed are uniformly selected to have matching properties in order to avoid any

mismatches. The values of these losses range between 0.01% up to 3% , in this study, a conservative value of 1% was assumed.

Soiling losses consider the amount of sunlight blocked by dirt accumulated on PV modules over time. It is affected by the amount of wind, nearby lands, local traffic, frequency and strength of rain. Typical values range from 1% to 5% (for long dry seasons), considering the characteristics of the location, a value of 2% is assumed. Proper service and cleaning maintenance can help reduce these losses.

Disorientation losses are losses that occur when the PV generator cannot be oriented or tilted at the optimal angles. These losses are assumed to be 0% due to the fact that the irradiation data obtained from Revit provide the value on the exact surface plane and therefore, taking into account disorientation losses.

Spectral and angular losses are due to the incidence of the irradiance which varies throughout the day and is not always perpendicular, and thus causing the module's power output to fall below the rated value. Values from 1 to 4 % were assumed , based on each PV generator setup.

Temperature losses occur due to the fact that under normal operating conditions, PV modules tend to operate at higher temperatures than the standard STC values. These losses are taken into account in this study, as seen earlier, in equations 3.5 and 3.6. Where peak power output is computed based on ambient temperature and manufacturer data. Nevertheless, these values were assumed to be 1% for all PV generators as an extra margin for error.

AC and DC wiring losses occur during the transmission of electrical energy from the photovoltaic modules to the grid or load.Factors such as cable length, cable size, and quality of connections can influence the magnitude of wiring losses, so it is important to minimize these losses by selecting appropriate cable sizes, optimizing cable routing, and ensuring reliable connections.A value of 2% of DC losses is suggested for most systems, and 1.5 % for AC losses. A conservative value of 4% for both DC and AC losses was taken into assumption for all generators.

Inverter losses occur during the conversion of DC electricity from solar panels to usable AC electricity. Conversion inefficiencies are caused by thermal losses, and auxiliary power consumption, therefore selecting high-quality inverters with high conversion efficiencies and effective thermal management systems can minimize these losses. Proper sizing also contributes to optimizing inverter performance and reducing energy losses in the system. The inverter selection process was based on fixed prerequisites. All selected inverters are three-phase, string inverters, grid-connected, and compatible with the local grid specifications ensuring stable and synchronized power output.

Inverter Selection

The selection of each inverter was based on the following criteria:

1- PV-to-Inverter sizing ratio R_S which is the ratio of the peak power of the PV generator measured in standard test conditions over the rated power of the inverter measured at the AC side. Simulations have shown that the optimal value of R_S is 1.2, however a range from 1 to 1.3 is acceptable. For that reason, the selection was based on the optimal value, but due to the variety of Watt peak generator powers, oversizing and undersizing values ranging from 1 to 1.3 were obtained for every area.

$$P_{inverter} = \frac{P_{PVG,}}{R_S} \quad \textbf{(Eq. 3.9)}$$

2-The MPPT input voltage range of the selected inverters should encompass both the highest and lowest values that the PV generator can provide at its maximum power point (MPP). This range is determined based on an irradiance of 1000 W/m2 and a temperature range spanning from -5 °C to +70 °C. These values are calculated from module specific temperature coefficients expressed following equations 3.10 and 3.11.

$$V_{MPP}(at - 5\ ^{o}C) = V_{MPP}(at\ STC) . (1 + k_T . (-5 - 25)) \quad \textbf{(Eq. 3.10)}$$

$$V_{MPP}(at\ 70\ ^{o}C) = V_{MPP}(at\ STC) . (1 + k_T . (70 - 25)) \quad \textbf{(Eq. 3.11)}$$

Where $\mathbf{k_t}$ is the voltage temperature coefficient provided by the module manufacturer.

3-The selected inverters must also withstand the maximum voltage generated by the PV generator under open circuit (OC) conditions, considering a cell temperature of -5 °C and an irradiance level of 1000 W/m2. Values are calculated from module specific temperature coefficients expressed following equation 3.12.

$$V_{OC}\ (at - 5\ ^{o}C) = V_{OC}(at\ STC) . (1 + k_T . (-5 - 25)) \quad \textbf{(Eq. 3.12)}$$

4- The chosen inverters have been carefully selected to withstand the maximum current generated by the PV generator under extreme operating conditions. This includes a cell temperature of +70 °C and an irradiance of 1000 W/m2. Current is calculated following equation 3.13.

$$I_{sc}(at\ 70\ ^{o}C) = I_{sc}(at\ STC) . (1 + k_T . (70 - 25)) \quad \textbf{(Eq. 3.13)}$$

The selected inverters all have rated european efficiencies above 97%, taking into account oversizing and undersizing, overall inverter losses are assumed to be ranging between 5 to 7%, for each PV generator depending on its sizing ratio.

AC-DC Cables selection:

Proper selection of DC and AC wires is crucial for efficient and safe operation of the building-integrated solar systems. They should be chosen based on their current-carrying capacity, voltage rating, and temperature rating to minimize power losses and ensure compatibility with the system's voltage and current requirements. The cabling sizing in this study was done for two main connections:

1-DC cables from PV Strings to Inverter inputs.

2- AC cables from Inverter to Breaker box (AC Load).

Windy Nation, suppliers of all kinds of equipment for solar and renewable energy systems, provided a simple conversion table for wire sizing, presented in figure 3.13 below. This conversion table gives the minimum cable cross section that can be used. The conversion gives the cable size in AWG (American Wire Gauge), which is a standard system used to specify the size of electrical wires. It assigns a numerical value to each wire gauge, with lower numbers representing thicker wires. The AWG wire rating indicates the wire's diameter or cross-sectional area, and then using table 3.2 provided by Kingsmill Industries , who are also cable suppliers, the nearest European standard cable cross-sectional area can be found.

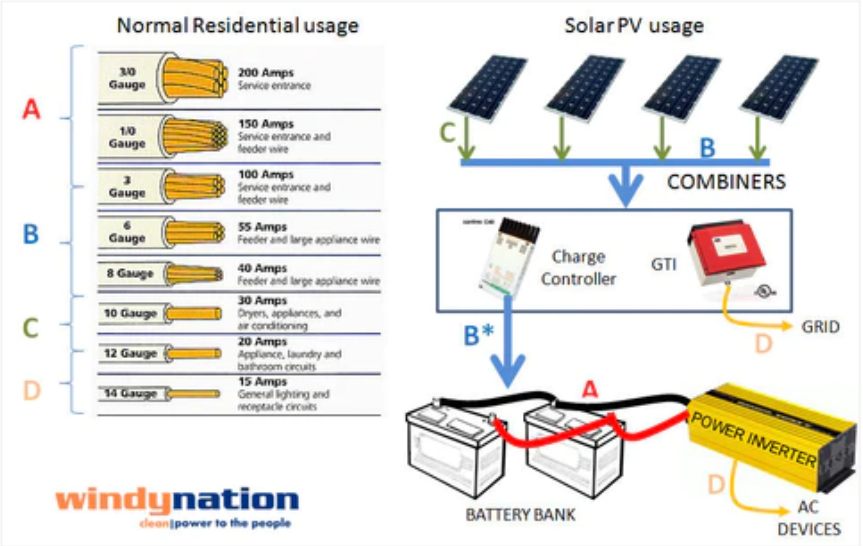

Figure 3.13 Cable sizing diagram based on current carrying capacity. (Source: Windy Nation) [48]

USA to European Cable Size Chart		
USA Standard Cable Size	**Equivalent Cross-Section**	**Nearest Available Cable Size**
20 AWG	0.519 mm2	0.5 mm2 - 0.75 mm2
18 AWG	0.823 mm2	1 mm2
16 AWG	1.31 mm2	1.5 mm2
14 AWG	2.08 mm2	2.5 mm2
12 AWG	3.31 mm2	4 mm2
10 AWG	5.26 mm2	6 mm2
8 AWG	8.37 mm2	10 mm2
6 AWG	13.3 mm2	16 mm2
4 AWG	21.15 mm2	25 mm2
2 AWG	33.62 mm2	35 mm2
1 AWG	42.41 mm2	50 mm2
1/0 AWG	53.49 mm2	70 mm2
2/0 AWG	67.23 mm2	70 mm2

Table 3.2 Cable size conversion table from AWG to EU standards. (Source: Kingsmill Industries) [49]

The voltage drop in cables is influenced by the length of the cable and its cross-sectional area. The lower, the more efficient the energy transmission is. Generally, longer cable lengths result in higher voltage drops due to increased resistance along the length of the cable, which is why it can be compensated by increasing the cross-sections of the cables which offer lower resistances. After having obtained the cross section of the wire from Table 3.2, the resistance of the wire in ohms/km can be found from table 3.3, provided by Engineeringtoolbox.com . The voltage drop

can then be calculated using equations 3.14 (for DC connections) and 3.15 (for 3-phase AC connections) below.

Cross Sectional Area (mm^2) (sq. in)	Resistance (ohm/km) (ohm/1000ft)	
	Copper	Aluminum
0.5	34.5	53
0.75	23	35.3
1.0	17.2	26.5
1.5	11.5	17.7
2.5	6.9	10.6
4.0	4.3	6.6
6.0	2.9	4.4
10	1.7	2.7
16	1.1	1.7
25	0.69	1.1
35	0.49	0.76
50	0.34	0.53
70	0.25	0.38
95	0.18	0.28
120	0.14	0.22
150	0.11	0.18
185	0.093	0.14
240	0.072	0.11
300	0.058	0.088
400	0.043	0.066
500	0.035	0.053
630	0.027	0.042

Table 3.3 Wire resistance in Ohms/km for different cable cross sections. [52]

$$V_{D,DC} = 2.\ R\ .\ L\ .\ I \qquad \text{For DC cables} \qquad \textbf{(Eq. 3.14)}$$

$$V_{D,AC} = \sqrt{3}.\ R\ .\ L\ .\ I \qquad \text{For 3-phase AC cables} \qquad \textbf{(Eq. 3.15)}$$

Where

- $\mathbf{V_D}$ is the voltage drop (V) .
- **R** is the resistance of the cable material in ohms per meter (Ω/m).
- **I** is the string current flowing through the cable in amperes (A).
- **L** is the length of the cable in meters (m).

Since the connection lengths are unknown, the lengths were assumed for each separate system and cable upsizing was done when necessary to maintain a voltage drop of below 2%, and thus enable more efficient power transmission.

The percentage of voltage drop is obtained using equations 3.16 and 3.17 below..

$$V_{D,\,DC}\,(\%) = \frac{V_{D,\,DC}}{V_{string}}$$ For DC cables (PV String to inverter input) **(Eq. 3.16)**

$$V_{D,\,AC}\,(\%) = \frac{V_{D,AC}}{V_{out}}$$ For AC cables (Inverter output to Breaker box) **(Eq. 3.17)**

Where

- $\mathbf{V_{string}}$ is the rated output voltage from the PV string in Volts (V).

- $\mathbf{V_{OUT}}$ is the rated output voltage of the inverter in Volts (V).

4. Results

The following section presents the results obtained from the implementation of each system designed for each of the 7 areas referred to in figure 3.5 from section 3.2 of this paper . It focuses on key aspects, including product selection, panel layout, and the energy output achieved in kilowatt-hours (kWh) according to all the criteria discussed in the Methodology section of this report.

According to the results obtained from the solar analysis presented in Table 4.1 below, it can be noted that the surfaces with the highest solar potential that will be considered for the study are the following:

-Area 1- High Roof
-Area 2- Terrasse-Balcony Railings
-Area 3- Facade 1-A
-Area 4- Facade 1-B
-Area 5- Facade 2

Other surfaces (Highlighted in Red in table 4.1) exhibit less than 35 % of the irradiation received on the surface with most potential, the high roof, and therefore, were not considered.

	Cumulative annual irradiation in kWh/m^2								
	High Roof	**High Roof -South Facing**	**Terrasse**	**Facade 1-A (SW)**	**Facade 1-B (SW)**	**Facade 2-Tilted (SE)**	**Facade 3 (NE)**	**Facade 4 (NW)**	**Terrasse-Balcony Railing**
Total yearly	1691	1762	562	1135	1102	928	373.12	610	1003

Table 4.1 Cumulative yearly irradiation in kWh/m^2.

4.1 High Roof

The high roof represents the surface with the highest solar and wind energy potential, and the only area when wind systems can be placed.

Figure 4.1 The roof of building 'I'.

After further analysis and market research in wind turbines, some of the products that were considered for roof mounting, such as the vertical axis mini wind turbine Aeolos-V , shown in figure 4.2 below, provided by manufacturers Aeolos wind turbines. These turbines come with a variety of rated power outputs ranging from 300 W to 3 kW, they can be well integrated on the roof and are quiet, safe, reliable and have a low start wind speed of 2 m/s. They can be used for the 120V off-grid application or 220V grid tie application and it is widely applied for small buildings, schools, supermarkets, homes and low noise areas.

Figure 4.2 Vertical Axis Wind Turbine with Roof Mounting. (Source: WindTurbineStar) [46]

However, based on the wind potential data obtained in the mounting area and the model's technical specifications, it was found that with a mean annual wind speed of 4.04 m/s at the location, the energy output of the 1 kW variant of the vertical axis mini wind turbine Aeolos-V 1kW was found to be around 1250 kWh per year as seen in figure 4.3 sourced from the product's technical sheet. Compared to solar systems, a highly efficient solar PV array can generate around 40 times this amount of energy per year, making the energy output of wind systems very low, even with the presence of multiple turbines, and therefore, it was concluded that the limited available area on the roof is better taken advantage of using solar systems, rendering wind systems unsuitable for our conditions. Higher power output products can be considered, but more power output means bigger size and dimensions, which can lead to questionable safety issues and non aesthetic building integration onto the building's roof.

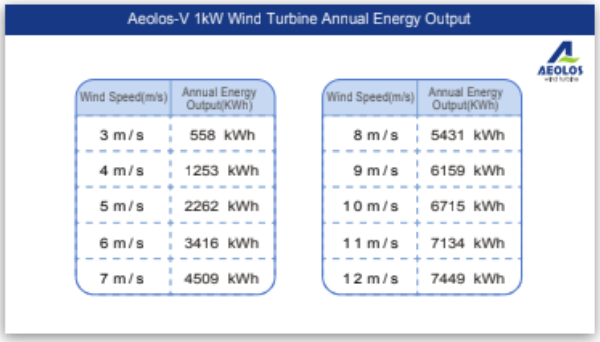

Figure 4.3 Aeolos-V 1 kW Energy output vs Annual average wind speed (m/s).

4.1.1 Available Area

The available space on the roof of building "I" is quite limited and its architecture is a bit complex. For that reason, an area of 10 x 35 m^2 was considered for the PV design. Due to lack of resources, this area was estimated using Google maps, but it was set conservatively while taking into account additional space for other activities. The considered area is shown in figure 4.1 above, highlighted in red.

4.1.2 Module

Since the high roof is the area where the most solar power can be harvested due to the facility of tilt and orientation configuration. To take advantage of that potential and the limited available roof space, a highly efficient solar module was selected for this area, which is the Tiger Neo N-type Monocrystalline bifacial module JKM580N-72HL4-BDV, from Jinko Solar. These modules can supply an output power of 580 W_P from the front side. Backside gains, which can reach 25 % of the front side gains, can increase peak power output up to 725 Wp.

In the study, the backside gain is assumed to be 5% , based on the reflectivity of the roof surface (Albedo), which can raise the output power to 609 Wp. Additionally, placing the modules on high structures improves the back side irradiance uniformity and leads to increased wind loads on the modules. The best yield results are obtained for ground clearances around 1.4 meters.

4.1.3 Configuration

To capitalize on the limited available roof space area, the number of panels had to be maximized, which meant finding the correct configuration. In the solar analysis in Revit, roof orientation was compared between exactly south oriented, which is optimal, and between being a little bit tilted towards the northwest in order to match the roof architecture and place more modules. The difference in irradiation was about 4 % less when the orientation matched the roof architecture but, the installation of more panels is possible and easier, which is why this orientation was adopted.

The tilt angle of the modules was set to be 39 ^{o}, which is obtained by subtracting 2.5 degrees from the latitude of the location (41.41^{o}). At this tilt angle setting, energy generation is maximized throughout the whole year. Taking into account the orientation and tilt angle, the minimal distance between rows was computed following Equation 3.1, and was found to be 5.8 meters.

With this configuration, a total of 54 panels can fit on the available area on the roof, laid out in 6 rows of 9 solar modules each.

Figure **4.4** High Roof panel configuration.

4.1.4 Inverter Selection

The selection of the inverter was based on the 4 criteria previously discussed in Section 3.3.2 under inverter selection. An intensive inverter market research led to the selection of the grid connected three-phase solar inverter provided by Huawei Technologies, the Huawei-SUN2000-30KTL-M3. This particular inverter was found to be the most suitable according to the criteria and has an efficiency of 98.4%, however, this selection yields a PV-to-Inverter sizing ratio R_s = 1.082 which is a bit off from the optimal 1.2 value but still considered within an acceptable range. That might lead to additional conversion inefficiencies, which is why inverter and MPPT losses were assumed to be 5 % in the losses table, table 4.2.

Furthermore, this inverter has 4 MPPT trackers with 2 string inputs for each, leading to a total of 8 strings inputs. In order for this inverter to withstand input voltages and the short circuit currents calculated in section 3.3.2 using equations 3.10, 3.11, 3.12, and 3.13, 3 of the 4 available MPPT trackers must be used for this array, with 2 strings of 9 modules connected to each MPPT.

4.1.5 Energy Yield

The Ross coefficient k, needed to compute the cell temperature with respect to the ambient temperature was assumed to have the value of 0.0208 $K.m^2$ / W based on table 3.1 from Section 3, which is the coefficient for free standing systems. The peak power output of a single module was then calculated for each month using Equation 3.6, multiplied by 54 panels to obtain the whole PV array output P_{PVG}.

The various losses in the system that indicate the Performance Ratio of the system are present in table 4.2 below.

High Roof Losses	Losses in percent (%)
Module Mismatch	1
Soiling	2
Spectral and angular	1
Temperature	1
DC-AC Wiring	4
Inverter	5
PR	0.86
PR Considered (+5% additional losses)	0.81

Table 4.2 System losses assumed and performance ratio for the roof.

Using equation 3.5, the energy output of this system is calculated and results are presented in table 4.3 below:

Area 1 : High Roof	Monthly Irradiation (Wh/m2)	F_S (Shadow losses)	PR	Peak Generator Power P_{PVG} (W_p)	Energy output E_M (kWh)
January	77000	1	0.81	33481.83473	2088.262032
February	109000	1	0.81	33120.32788	2924.193749
March	144000	1	0.81	32788.72321	3824.476675
April	169000	1	0.81	32444.26628	4441.295611

May	176000	1	0.81	32204.3433	4591.051182
June	192000	1	0.81	31771.19723	4941.056594
July	198000	1	0.81	31721.26275	5087.456119
August	179000	1	0.81	31719.65253	4599.03242
September	146000	1	0.81	31941.84294	3777.442346
October	133000	1	0.81	32130.99225	3461.471795
November	90000	1	0.81	32881.68878	2397.075112
December	78000	1	0.81	33318.06485	2105.035337
Total	**1691000**	**1**	**0.81**	**32460.34973**	**44237.84897**

Table 4.3 Energy Output in kWh of Roof PV system.

As can be seen from the results obtained in Table 4.3, this PV generator design on the roof, with all the losses and assumptions taken into account, can generate up to 44.23 MWh of electricity per year.

4.1.6 Cable sizing

According to the criteria discussed in section 3.3.2 under AC- DC cables, the results obtained for the cable sizing for this area's system are shown in table 4.4 below.

High Roof	Current I (A)	Cable cross section (mm2)	Assumed length (km)	Resistivity (ohm/km)	V drop (V)	V drop (%)
For DC cables (PV String to inverter input)	14.66	4	0.03	4.3	3.78	0.76
For AC cables (Inverter output to Breaker box)	**47.9**	**16**	**0.02**	**1.1**	**1.825**	**0.83**

Table 4.4 DC-AC cables with corresponding voltage drop.

The required cable cross-sections are selected based on their current carrying capacity and a cable length was assumed for each connection. The resistivity in the wire obtained is for copper wire, as they provide less resistance than aluminum. Based on the assumptions, the resulting voltage drop is below 1% for both connections, which falls in the acceptable range.

4.2 Facade 1 (A & B)

According to the irradiation results obtained from table 4.1, between all the facades, Facade 1 has the highest yearly potential for PV generation. As this facade has two faces with different orientations, the study took each face individually thus creating two different areas Facade 1- A and facade 1-B, as shown in figure 4.5 below.

Figure 4.5 Facade 1 sides A & B.

4.2.1 Available Area

The available area for both faces of facade 1 was obtained from measurements taken on site. On face A of the facade, the total available area for PV integration was found to be 15 x 9.8 m^2, while face B had an available area of 20 x 22 m^2, allowing plenty of room for integration on that facade. These dimensions were set with a small tolerance of measurement and approximation errors taken into account.

4.2.2 Module selection

To take advantage of the solar potential of this facade, the same highly efficient solar module was selected for both faces, which is the Tiger Neo N-type Monocrystalline monofacial module JKM585N-72HL4-V, from Jinko Solar. These modules can supply an output power of 585 W_P with an efficiency of 22.6 %. Multiple modules were tested for that surface, but the selected model demonstrated the highest energy output between all.

4.2.3 Configuration

On this surface, since the modules will be facade integrated, the orientation cannot be manipulated and thus the module orientation has to match that of the surface. Furthermore, for a smoother integration, tilt angles cannot be changed and remain at 90°, just like the facade.

With this setup, a total number of 52 panels can fit onto surface 1-A , laid out in 4 rows of 13 panels each and a total of 153 panels onto surface 1-B, laid out in 9 rows of 17 panels each. This configuration also takes into account a bit of additional space between the rows in order to facilitate maintenance and/or installation activities. Layout is presented in figure 4.6 below.

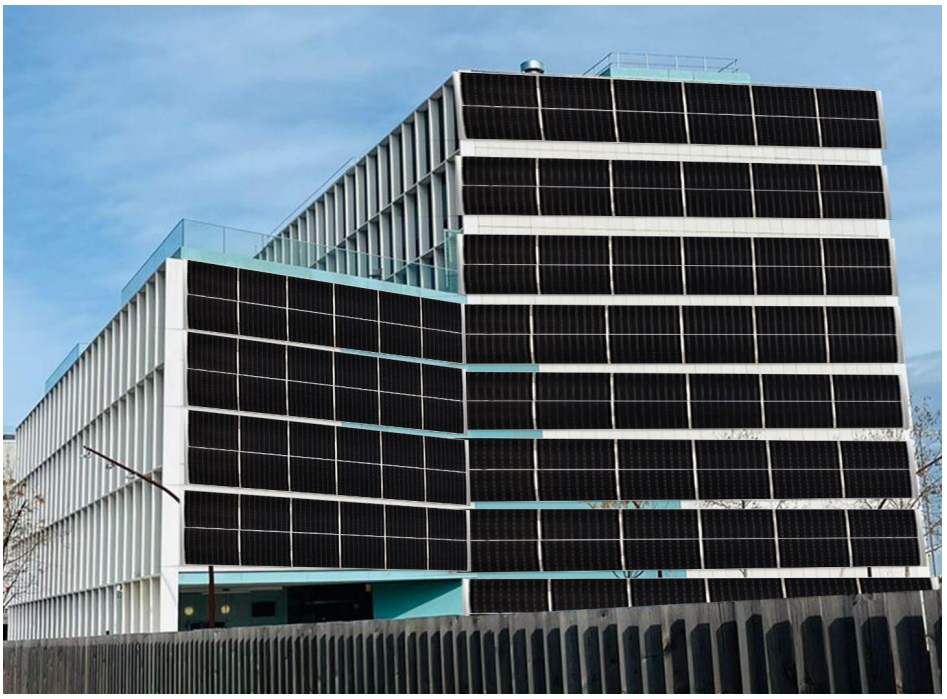

Figure 4.6 Visualization of layout on Facade 1.

4.2.4 Inverter Selection

Due to differing solar irradiance on the two faces of facade 1, an inverter was selected for each one of them to avoid any generation mismatch and induce losses.

For Face A, the most suitable and efficient inverter was the Solax X3-PRO G2-25. It is also a grid connected three-phase solar inverter provided by manufacturers Solax Power. It has an efficiency of 98 % and with a rated power output of 25 kW, the PV-to-Inverter sizing ratio R_s = 1.15 which is in the acceptable range and not too far off the optimal 1.2 value. Inverter and MPPT losses were also assumed to be 5%. Furthermore, this inverter has 2 MPPT trackers with 2 string inputs for each, leading to a total of 4 string inputs. In order for this inverter to withstand input voltages and the short circuit currents calculated in section 3.3.2, all 4 strings were used with 13 panels per string.

For Face B, due to the high PV generator power output and long strings, two inverters were selected for that surface in order to minimize losses. One for 78 of the modules available, and the other one for the remaining 75. As power output of both arrays is relatively close, the same model of inverter was used, which is the Huawei- SUN2000-36KTL-M3 from Huawei technologies.It is also a grid connected three-phase solar inverter, with an efficiency of 98.4 %. A rated power output of 36 kW indicated the PV-to-Inverter sizing ratio R_s = 1.16 (for 75 panels) and R_s = 1.206 (for 78 panels) which are in the acceptable range and close to the optimal value of 1.2.
Inverter and MPPT losses were also assumed to be 5% for these generators.

Furthermore, this inverter has 4 MPPT trackers with 2 string inputs for each, leading to a total of 8 string inputs. In order for this inverter to withstand input voltages and the short circuit currents calculated in section 3.3.2, 3 of the 4 MPPT trackers are used with the 75 panels connected to 6 string inputs of the inverter with 3 strings having 12 modules each and 3 strings having 13 modules each and every MPPT input having a total of 25 panels connected to it.
The remaining 78 panels are also connected to 3 out of 4 MPPT inputs of the other inverter, using 6 strings with 13 modules per string.

4.2.5 Energy Yield

The Ross coefficient k, needed to compute the cell temperature with respect to the ambient temperature was assumed to have the value of 0.0538 $K.m^2 / W$ based on table 3.1 from Section 3, which is the coefficient for facade integrated systems. The peak power output of a single module was then calculated for each month using Equation 3.6, and multiplied by 52 panels to obtain the whole PV array output P_{PVG} on face A and by 153 panels to obtain the output of face

B. The various losses in the system that indicate the Performance Ratio of each face were assumed to be identical and are presented in table 4.5 below.

Losses	Losses in percent (%)
Module Mismatch	1
Soiling	2
Spectral and angular	2.5
Temperature	1
DC-AC Wiring	4
Inverter	5
PR	0.845
PR Considered (+5% additional losses)	0.795

Table 4.5 System losses assumed and performance ratio for Facade 1 PV systems.

Using equation 3.5, the energy output of each system is calculated and results are presented in tables 4.6 and 4.7 below:

Area 3: Facade 1-A	Monthly Irradiation (Wh/m2)	F_S (Shadow losses)	PR	Peak Generator Power P_{PVG} (W_p)	Energy output E_M (kWh)
January	84000	1	0.795	29252.8581	1953.505864
February	103000	1	0.795	28876.50973	2364.552999
March	109000	1	0.795	29077.23382	2519.687697
April	100000	1	0.795	29277.17591	2327.535485
May	82000	1	0.795	29530.73364	1925.108526
June	78000	1	0.795	29333.43708	1818.966433
July	86000	1	0.795	29209.19372	1997.032575
August	95000	1	0.795	28918.16676	2184.044544
September	101000	1	0.795	28592.84006	2295.862093
October	116000	1	0.795	28031.84072	2585.096351
November	94000	1	0.795	28502.2857	2129.97581
December	87000	1	0.795	28874.65077	1997.115221

Total	**1135000**	**1**	0.795	**28956.4105**	**26098.4836**

Table 4.6 Energy Output in kWh of Facade 1-A PV system.

Area 4: Facade 1-B	Monthly Irradiation (Wh/m2)	F_S (Shadow losses)	PR	Peak Generator Power P_{PVG} (W_p)	Energy output E_M (kWh)
January	70000	1	0.795	86070.9094	4789.846108
February	85000	1	0.795	84963.5767	5741.413696
March	102000	1	0.795	85554.16875	6937.587544
April	102000	1	0.795	86142.45989	6985.292072
May	95000	1	0.795	86888.50474	6562.25432
June	98000	1	0.795	86307.99755	6724.256089
July	104000	1	0.795	85942.43537	7105.720557
August	102000	1	0.795	85086.1445	6899.635457
September	97000	1	0.795	84128.93326	6487.602689
October	100000	1	0.795	82478.30058	6557.024896
November	77000	1	0.795	83862.49445	5133.642598
December	70000	1	0.795	84958.10708	4727.918659
Total	**1102000**	**1**	0.795	**85198.66936**	**74652.19468**

Table 4.7 Energy Output in kWh of Facade 1-B PV system.

The results provided in tables 4.6 and 4.7, show that Facade 1-A and Facade 1-B can generate respectively up to 26 MWh and 74.6 MWh yearly, leading to a total energy generation of up to 100 MWh per year from this one facade.

4.2.6 Cable sizing

According to the criteria discussed in section 3.3.2 under AC- DC cables, the results obtained for the cable sizing for the systems of facade 1-A and 1-B are shown respectively , in tables 4.8 and 4.9 below.

Facade 1-A	Current I (A)	Cable cross section (mm2)	Assumed length (km)	Resistivity (ohm/km)	V drop (V)	V drop (%)
For DC cables (PV String to inverter input)	**14.84**	**4**	**0.03**	**4.3**	**3.83**	**0.535**

For AC cables (Inverter output to Breaker box)	**41.8**	**16**	**0.02**	**1.1**	**1.6**	**0.724**

Table 4.8 DC-AC cables with corresponding voltage drop.

Facade 1-B	**Current I (A)**	**Cable cross section (mm2)**	**Assumed length (km)**	**Resistivity (ohm/km)**	**V drop (V)**	**V drop (%)**
For DC cables (PV String to inverter input)	**14.84**	**4**	**0.03**	**4.3**	**3.83**	**0.535**
For AC cables (Inverter output to Breaker box)	**58**	**30**	**0.02**	**0.59**	**1.185**	**0.539**

Table 4.9 DC-AC cables with corresponding voltage drop.

The required cable cross-sections are selected based on their current carrying capacity and a cable length was assumed for each connection. The resistivity in the wire obtained is for copper wire, as they provide less resistance than aluminum. Based on the assumptions, the resulting voltage drop is below 1% for both connections, which falls in the acceptable range.

4.3 Facade 2

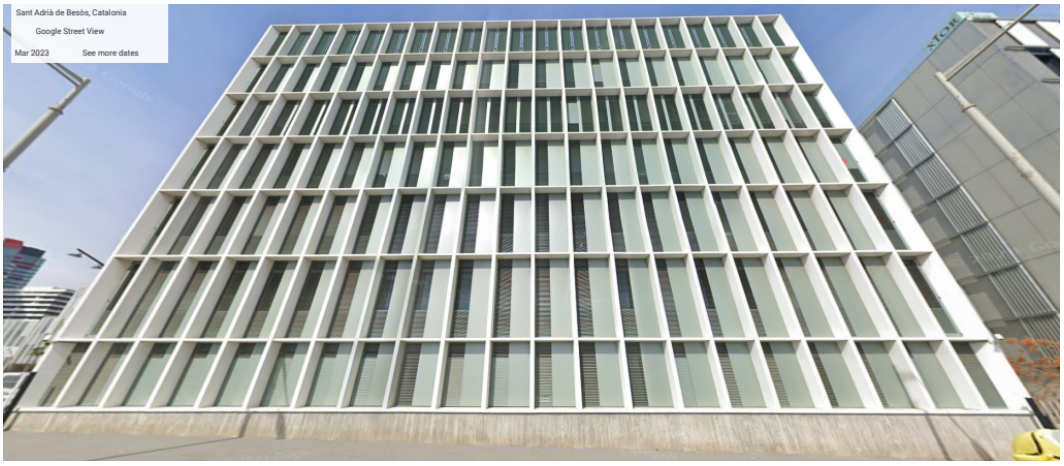

Figure 4.7 Facade 2

4.3.1 Area

As can be seen from figure 4.7 above, this facade entirely consists of a grid of windows of 7 rows and 19 blocks per row with a certain depth. As approximately half of the plane inside each block of the grid has a solid opaque region that is useless, these surfaces can be taken advantage of by placing PV modules onto them. With the dimensions measured on site, it could be established that 1 PV module can be fitted into each block, and since one of the grid rows does not have the solid opaque region, it will not be considered for the application, which leads to a total of 6 x 19 = 114 panels installed on this facade.

4.3.2 Module

Taking into consideration space restrictions, a different range of PV modules could be installed inside each block and the dimensions of the modules were irrelevant for the number of panels that can be installed, which is the same total of 114 panels can be installed regardless of the dimensions. For that reason,a highly efficient module was selected to maximize solar gains on that particular surface, which is the Tiger Neo N-type Monocrystalline monofacial module JKM630N-78HL4 provided by Jinko Solar. These modules can supply an output power of 630 W_P with an efficiency of 22.54 %.

4.3.3 Configuration

On this surface, the modules will be covering the opaque part of each block of the grid. To make use of the space, the panels are oriented more towards the south and are set up diagonally to cover the opaque region without covering the sunblind part. This module plane was drawn and designed on the Revit Software and irradiation values taken were obtained on that plane exactly.

With this setup, a total number of 114 panels can fit onto the facade, laid out in 6 rows of the grid with 19 modules, one in each block of each row. The layout is demonstrated in figures 4.8 and 4.9 below.

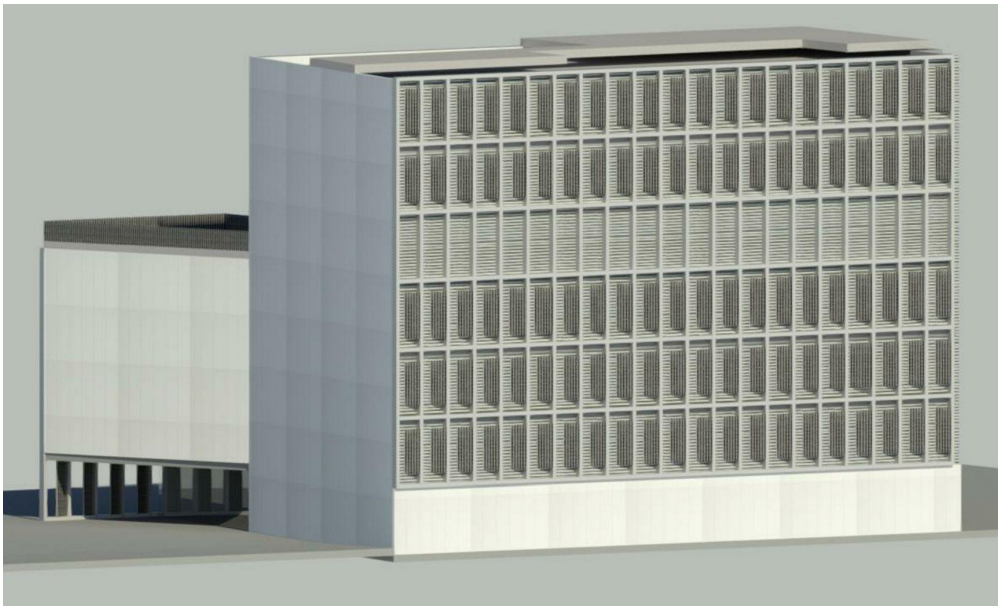

Figure 4.8 Visualization of layout on Facade 2.

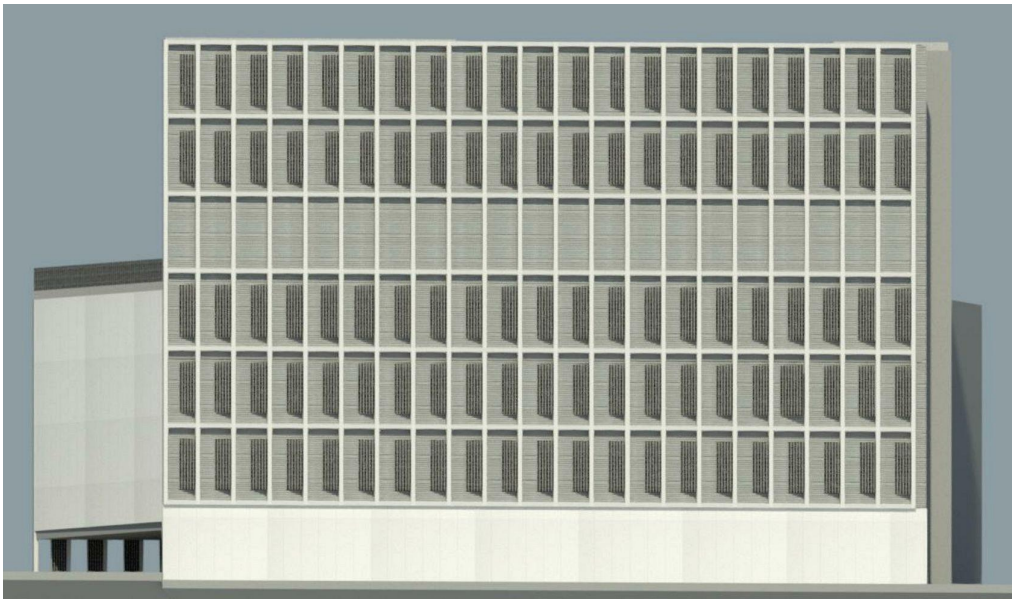

Figure 4.9 Visualization of layout on Facade 2

4.3.4 Inverter Selection

To efficiently convert the DC power generated by the system on this facade, another inverter from Huawei Technologies was selected, which is the SUN2000-60KTL-M0. With an efficiency of 98.5%, this inverter provides an output power of 60 kW yielding a sizing ratio of Rs = 1.1, which is also in the acceptable range.

With 6 MPPT trackers and 2 string inputs for each, every MPPT is connected to 19 modules in total, split in two strings with 9 modules per one string and 10 modules per the other. Inverter and MPPT losses were also assumed to be 5% for these generators.

4.3.5 Energy Yield

The Ross coefficient k, needed to compute the cell temperature with respect to the ambient temperature was assumed to have the value of 0.0342 $K.m^2 / W$ based on table 3.1 from Section 3, which is the coefficient for not so well cooled systems. The peak power output of a single module was then calculated for each month using Equation 3.6, and multiplied by 114 panels to obtain the whole PV array output P_{PVG} on facade 2.

The various losses in the system that indicate the Performance Ratio of the system are present in table 4.10 below.

Losses	Losses in percent (%)
Module Mismatch	1
Soiling	1
Spectral and angular	4
Temperature	1
DC-AC Wiring	4
Inverter	5
PR	0.84
PR Considered (+5% additional losses)	0.79

Table 4.10 System losses assumed and performance ratio for Facade 2 PV systems.

Using equation 3.5, the energy output of each system is calculated and results are presented in table 4.11 below:

Area 5: Facade 2	Monthly Irradiation (Wh/m2)	F_S (Shadow losses)	PR	Peak Generator Power P_{PVG} (W_p)	Energy output E_M (kWh)
January	64000	1	0.79	72321.96396	3656.598498

February	81000	1	0.79	71716.88322	4589.163357
March	83000	1	0.79	71800.63015	4707.967319
April	83000	1	0.79	71527.84277	4690.08065
May	73000	1	0.79	71355.13033	4115.050366
June	72000	1	0.79	70633.13338	4017.612627
July	79000	1	0.79	70254.69005	4384.595206
August	84000	1	0.79	69927.32907	4640.377557
September	82000	1	0.79	70006.84015	4535.043105
October	91000	1	0.79	69801.78618	5018.050408
November	69000	1	0.79	71140.38603	3877.862443
December	67000	1	0.79	71777.43884	3799.179838
Total	**928000**	**1**	0.79	**71022.00451**	**52031.58137**

Table 4.11 Energy Output in kWh of Facade 2 PV system

As can be seen from the results obtained in table 4.11, this PV generator design on facade 2, with all the losses and assumptions taken into account, can generate up to 52 MWh of electricity per year.

4.3.6 Cable sizing

According to the criteria discussed in section 3.3.2 under AC- DC cables, the results obtained for the cable sizing for this area's system are shown in table 4.12 below.

Facade 2	Current I (A)	Cable cross section (mm2)	Assumed length (km)	Resistivity (ohm/km)	V drop (V)	V drop (%)
For DC cables (PV String to inverter input)	**14.68**	**4**	**0.03**	**4.3**	**3.78**	**0.63**
For AC cables (Inverter output to Breaker box)	**173**	**95**	**0.02**	**0.18**	**1.079**	**0.49**

Table 4.12 DC-AC cables with corresponding voltage drop.

The required cable cross-sections are selected based on their current carrying capacity and a cable length was assumed for each connection. The resistivity in the wire obtained is for copper wire, as

they provide less resistance than aluminum. Based on the assumptions, the resulting voltage drop is below 1% for both connections, which falls in the acceptable range.

4.4 Terrasse Balcony Railing

While examining the irradiation results obtained from Revit, simulations were made on the terrasse that is located on the 4 the floor of the building, where balcony railings are available. And irradiation results on the railings that are facing south prevailed that they are subjected to a decent amount of yearly radiation compared to other surfaces, as can be seen previously in table 4.1 .

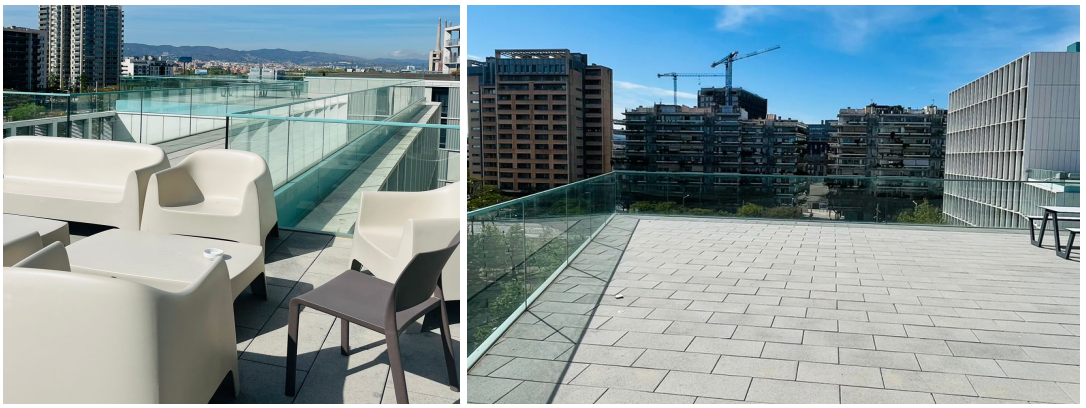

Figure 4.10 Terrasse area with balcony railings.

4.4.1 Area

In order to compute the available area for PV modules, on-site measurements were taken for all the balcony railings widths that are south facing, and with that data, the number of modules to be installed was determined.

4.4.2 Module

Only in this part of the design, a fully building integrated PV module was considered. Provided by manufacturers SolarInnova, the model SI-ESF-M-BIPV-BL-RL-M156-4 demonstrated in figure 4.11 was selected for the application, which is a transparent PV module that is designed to replace traditional passive balcony railings while maintaining architectural integrity. These modules have a peak power output of 222 W and an efficiency of 17.63%. With the area restrictions taken into account, the total number of modules that can be installed to replace the traditional glass railings was found to be 42 in total.

Figure 4.11 Terrasse BIPV balcony module.

4.4.3 Configuration

The configuration of these modules is restricted to the already existing railings, therefore, orientation and tilt angles are not configurable.

4.4.4 Inverter Selection

To efficiently convert the DC power generated by the system, another inverter from Solax Power was used, which is the X3-MIC G2- 8K. With an efficiency of 97.8 %, this inverter provides an output power of 8 kW yielding a sizing ratio of Rs = 1.11, which falls in the acceptable range. It has 2 MPPT trackers with 1 string input each, meaning the 1 string of 21 modules is connected to each MPPT. Inverter and MPPT losses are assumed to be 5% for this system.

4.4.5 Energy Yield

The Ross coefficient k, needed to compute the cell temperature with respect to the ambient temperature was assumed to have the value of 0.0455 $K.m^2 / W$ based on table 3.1 from Section 3, which is the coefficient for transparent PV systems. The peak power output of a single module was then calculated for each month using Equation 3.6, and multiplied by 42 panels to obtain the whole PV array output P_{PVG}.

The various losses in the system that indicate the Performance Ratio of the system are present in table 4.13 below.

Losses	Losses in percent (%)
Module Mismatch	1
Soiling	1
Spectral and angular	4
Temperature	1
DC-AC Wiring	4
Inverter	5
PR	0.84
PR Considered (+5% additional losses)	0.79

Table 4.13 System losses assumed and performance ratio for balcony railing system.

Using equation 3.5, the energy output of each system is calculated and results are presented in table 4.14 below:

Area 2 : Terrasse Balcony	Monthly Irradiation (Wh/m2)	F_S (Shadow losses)	PR	Peak Generator Power P_{PVG} (W_p)	Energy output E_M (kWh)
January	61000	1	0.79	9250.778966	445.7950384
February	81000	1	0.79	9031.098495	577.8999927
March	97000	1	0.79	8942.080405	685.2316215
April	95000	1	0.79	8933.441268	670.4547672
May	83000	1	0.79	8965.570365	587.8724488
June	82000	1	0.79	8818.746476	571.2783967
July	89000	1	0.79	8755.355483	615.589044
August	93000	1	0.79	8657.452921	636.0630661
September	92000	1	0.79	8604.301213	625.3606121
October	95000	1	0.79	8537.205423	640.717267
November	72000	1	0.79	8866.781911	504.3425551
December	63000	1	0.79	9114.442066	453.6257816
Total	**1003000**	**1**	0.79	**8873.104583**	**7014.230591**

Table 4.14 Energy Output in kWh of balcony railing PV system.

As can be seen from the results obtained in Table 4.14, this balcony railing PV generator design on the terrasse, with all the losses and assumptions taken into account, can generate up to 7 MWh of electricity per year.

4.4.6 Cable sizing

According to the criteria discussed in section 3.3.2 under AC- DC cables, the results obtained for the cable sizing for this area's system are shown in table 4.15 below.

Terrasse Balcony	Current I (A)	Cable cross section (mm2)	Assumed length (km)	Resistivity (ohm/km)	V drop (V)	V drop (%)
For DC cables (PV String to inverter input)	**10.2**	**2.5**	**0.03**	**6.9**	**4.22**	**0.64**
For AC cables (Inverter output to Breaker box)	**12.8**	**2.5**	**0.02**	**6.9**	**3.06**	**1.39**

Table 4.15 DC-AC cables with corresponding voltage drop.

The required cable cross-sections are selected based on their current carrying capacity and a cable length was assumed for each connection. The resistivity in the wire obtained is for copper wire, as they provide less resistance than aluminum. Based on the assumptions, the resulting voltage drop is below 2% for both connections, which falls in the acceptable range.

4.5 Total Yield

By summing all these systems together, the total yield can be obtained giving an indication of how much of the campus and building consumption can all these systems offset based on the building demand data provided in section 3.1.2 of this study. Results are shown in table 4.16 below.

Month	Energy Produced (kWh)	Energy Saved from Campus(%)	Energy Saved from Building (%)
January	12934.00754	5.495647988	32.32734111
February	16197.22379	6.494241905	38.20142297
March	18674.95086	6.392947664	37.60557449
April	19114.65859	7.582443874	44.60261102

May	17781.33684	5.979452421	35.17324954
June	18073.17014	6.421609399	37.77417293
July	19190.3935	7.039091466	41.40642039
August	18959.15304	10.94443434	64.37902551
September	17721.31084	6.470111117	38.05947716
October	18262.36072	6.310247373	37.1191022
November	14042.89852	5.027278641	29.5722273
December	13082.87484	5.378078391	31.63575524
Total	**204034.3392**	**6.498856815**	**38.2285695**

Table 4.16 Overall monthly systems production and energy saved from campus and building.

As can be seen from table 4.16, the results of the study demonstrate the significant energy production achieved through the integration of solar systems on various surfaces of the building. The combined output of all the systems amounted to 204,034 kWh, and with the assumption that the building represents 17% of the whole campus consumption, the overall systems output results remarkable energy savings of 6.49% of the overall campus consumption and an impressive 38.22% reduction in the building's energy consumption. These results highlight the effectiveness of the implementation of solar systems on different surfaces of the building and showcase their potential for widespread adoption.

5. Environmental Study

The environmental impact analysis conducted in this study focuses on assessing the reduction in carbon dioxide emissions resulting from the implementation of the PV systems. According to the practical guide for calculating greenhouse gas (GHG) emissions provided by Generalitat de Catalunya [50], it is estimated that each kilowatt-hour (kWh) of grid electricity contributes approximately 273 grams of CO2 emissions, while electricity sourced from renewable energy systems generates zero emissions.

To evaluate the long-term environmental benefits, the energy output of the solar systems designed in this project was analyzed over a 30-year lifespan. The selected product manufacturers guarantee a 30-year operational lifespan and provide information on linear performance degradation in the product's data sheet. Taking into account the degradation and annual energy loss factors, the PV systems implemented in this project have successfully avoided up to 1,553 tons of CO2 emissions over the 30-year period. This achievement represents a substantial reduction in greenhouse gas emissions, highlighting the positive environmental impact of the project.

Table 5.1 below presents the avoided CO2 for each of the systems installed individually.

Emissions Factor (grams of CO2/kWh)	273	
Area	**Energy Produced over 30 years (MWh)**	**Tons of CO2 avoided over 30 years**
High Roof	1,236.89	337.67
Facade 1-A	729.71	199.21
Facade 1-B	2087.27	569.82
Facade 2	1454.80	397.16
Terrasse Balcony	182.51	49.82
Total	**5,691.19**	**1,553.69**

Table 5.1 CO2 emissions avoided in tons.

6. Economic analysis

The economic analysis of the project involves a comprehensive assessment of the costs and financial aspects associated with the implementation of the selected solar systems. A market research was conducted to gather pricing information for the various equipment used. The prices of the equipment were gathered from direct contact with suppliers in Spain, and based on online markets , cost estimation was done and detailed information is provided in the annex section A2.

Table 6.1 below summarizes the total cost of resources, which includes module prices, inverter prices, and installation costs. Installation costs were assumed to be 20 % of the total equipment's price and the yearly maintenance cost was assumed to be 1.5%.

Summary	
Total cost of resources (€)	121,075
Total yearly maintenance (€)	1,513.44

Table 6.1 Summary of the costs of all systems.

To evaluate the economic viability of the project, the total costs, including equipment, installation, and maintenance expenses, were computed over the projected 30-year lifespan of the systems. The energy output generated by the solar systems over this period was calculated, taking into account any performance degradation. Over the 30 year life span, the total energy produced by all the systems installed averages around 189.706 MWh. According to insights provided by the UPC sustainability department presented in figure 6.1, the average tariff of electricity for the university over the past 6 years has been around 0.0665 €/kWh. With that tariff considered over the evaluation period, table 6.2 presents the total yearly revenue over the first 11 years of operation.

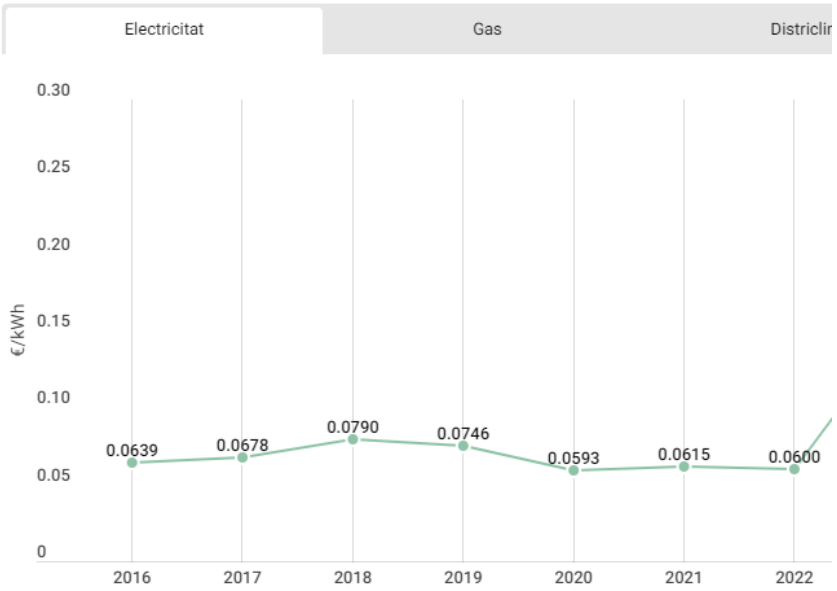

Figure 6.1 Evolution of electricity prices at UPC. (Source: UPC Sostenible) [51]

Year	Yield (kWh)	Price of electricity (€/ kWh)	Maintenance Yearly (€)	Annual Savings (€)	Balance (€)
1	201,853	0.0665	1,513.44	11,909.83	-109,165.36
2	201,015	0.0665	1,513.44	11,854.12	-97,311.24
3	2001,78	0.0665	1,513.44	11,798.41	-85,512.83
4	199,340	0.0665	1,513.44	11,742.70	-73770.13
5	198,502	0.0665	1,513.44	11,687	-62,083.13
6	197,665	0.0665	1,513.44	11,631.28	-50,451.85
7	196,827	0.0665	1,513.44	11,575.57	-38,876.28
8	195,989	0.0665	1,513.44	11,519.86	-27,356.42
9	195,151	0.0665	1,513.44	11,464.15	-15,892.26
10	194,314	0.0665	1,513.44	11,408.47	-4,483.82
11	193,476	0.0665	1,513.44	11,352.73	6,868.91

Table 6.2 Total yearly revenue from all PV Systems over an 11 year period.

Payback period and Return on Investment (ROI)

The payback period and return on investment (ROI) are crucial financial indicators to assess the viability and profitability of the solar project. Analysis of the data presented in Table 6.2 reveals that at the end of year 11, the project starts generating profits that exceed the initial investment cost. This is evidenced by the savings amounting to € 6,868.91. The balance at year 0 represents the total cost of resources, including equipment and installation, as shown in Table 6.1, totaling -€121,075.2 and then the annual resulting savings are added to that amount, maintenance costs deducted.

Beyond year 11, the project consistently generates substantial savings, averaging around €10,500 Euros per year. Over the 30-year duration, the cumulative savings reach an impressive amount of 211,986 €, as illustrated in Table 6.3. These figures highlight the financial success and long-term profitability of the solar project, demonstrating its ability to generate significant returns on the initial investment.

Year	Yield (kWh)	Price of electricity (€/ kWh)	Maintenance Yearly (€)	Annual Savings (€)	Balance (€)
27	180,0724	0.0665	1166.94	10,807	**180,936.12**
28	179,234	0.0665	1166.94	10,752	**191,341.79**
29	178,396	0.0665	1166.94	10,696	**201,691.74**
30	177,559	0.0665	1166.94	10,640	**211,986**

Table 6.3 Total Balance in Euros over a 30 year period.

The payback period, which is the time required for the project to recoup the initial investment, is estimated by examining the point at which the cumulative savings surpass the initial cost. In this case, it is evident that by the end of year 11, the project has generated sufficient savings to cover the initial investment.

The return on investment (ROI) serves as a compelling indicator of the project's profitability. By evaluating the ratio of net profit to the initial investment, the ROI was computed to be 194% according to Equation 6.1. This substantial ROI reflects the favorable financial performance of the project.

$$ROI\ (\%) = \frac{211{,}986\ (€)}{121{,}075\ (€)} = 175.08\ \% \qquad \text{(Eq. 6.1)}$$

Overall, the project demonstrates profitability in its entirety. However, it is essential to consider the profitability of each PV system in their respective areas as certain systems yield lower profits compared to others. Therefore, a comprehensive economic evaluation of each PV system is presented in tables below 6.4 to 6.8 below

Area 1: High Roof

Total Cost (€)	14,107
Total Yield (kWh)	1,236,890
Cost per Yield (€/kWh)	0.0114
Payback Period	6 Years
ROI (30 year period)	445.55 %

Table 6.4 High roof generated electricity cost in €/kWh.

Area 3: Facade 1-A

Total Cost (€)	12,345
Total Yield (kWh)	729,713
Cost per Yield (€/kWh)	0.017
Payback Period	9 Years
ROI (30 year period)	255 %

Table 6.5 Facade 1-A generated electricity cost in €/kWh.

Area 4: Facade 1-B

Total Cost (€)	34,358
Total Yield (kWh)	2,087,275
Cost per Yield (€/kWh)	0.0164
Payback Period	8 Years
ROI (30 year period)	266.48 %

Table 6.6 Facade 1-B generated electricity cost in €/kWh.

Area 5: Facade 2

Total Cost (€)	25,584
Total Yield (kWh)	1,454,803
Cost per Yield (€/kWh)	0.0175
Payback Period	9 Years
ROI (30 year period)	240.6 %

Table 6.7 Facade 2 generated electricity cost in €/kWh.

Area 2: Balcony Terrasse

Total Cost (€)	34,680
Total Yield (kWh)	182,511
Cost per Yield (€/kWh)	0.19
Payback Period	95 Years +
ROI (30 year period)	-72.27 %

Table 6.8 Balcony Terrasse generated electricity cost in €/kWh.

Values of the cost of the electricity generated by each system obtained in these tables are compared with the average tariff for campus electricity 0.0665 €/kWh presented in figure 6.1, and cost savings vary between 73% obtained from facade 2 and 82.8% from the roof system which offers the highest percentage. All systems prove to be profitable and financially advantageous, except for the balcony terrace system, where the cost of the electricity produced is 240.6 % the tariff for campus electricity.

While the balcony system seems unprofitable, it is to consider that the modules installed in that area are designed for building integration, which means that they are replacing actual construction elements of the building such as, in this case, traditional glass balcony railings. The true cost of this system must deduct the cost of the construction elements. In addition, It is important to note that while building-integrated photovoltaic (BIPV) elements offer the advantage of seamlessly integrating solar panels into the building's architecture, they can also present challenges in terms of efficiency. They are often constrained by factors such as limited surface area and architectural suitability.

In addition, all the values obtained in this section do not include governmental incentives or subsidies for installation discussed in section 2.6.

7. Conclusions

7.1 Results discussions

The conclusions drawn from the research and analysis conducted in this study provide valuable insights into the feasibility and effectiveness of integrating solar systems in the building design. The implementation of solar systems has demonstrated significant energy production capabilities and a substantial contribution to reducing carbon dioxide (CO2) emissions, which is a relevant target in all European institutions and enterprises.

Although the high roof is the area with the highest solar energy production potential and its system yields the highest return on investment, the systems installed on facades 1 and 2 combined were able to generate 245.36 % more energy, but for lower economic return, that is still profitable. This significant difference can be attributed to the limitations posed by the available area on the roof, which emphasizes the importance of utilizing all viable surfaces for solar integration. It is important to note that the most efficient available equipment was selected for all the systems and the results obtained can represent the maximum amount of savings in electricity consumption that can be reached by the implementation of these systems, however, it is crucial to ensure that these systems comply with local regulations and necessary permits can be obtained for their installation.

Furthermore, challenges may arise with the installation process of facade systems. As these systems are being implemented on an already existing building, they would have to be attached onto the facade's already existing architecture which may add some complexities, as in the case of Facade 2 from Area 5, where the grid pattern is present and achieving an aesthetically appealing installation with proper cable and connection management might present some difficulties. For this reason, proper planning and coordination with experienced professionals are necessary to overcome these challenges and ensure a seamless and visually appealing integration of the systems.

On the other hand, the use of BIPV systems in the design demonstrated to be non-profitable due to its low energy yields and high equipment costs. Although less efficient, the cost of the BIPV balcony railings modules selected for the terrasse were about 3.5 times more expensive than highly efficient traditional solar modules and that may be due to the specialized design and integration requirements which often entail additional expenses for customization and installation. However, as mentioned earlier in the economic analysis, BIPV systems are designed to

replace traditional building elements, and their cost should offset the cost of these elements which might make BIPV systems more profitable if efficiently integrated.

Last but not least, to ensure the long-term effectiveness and reliability of the solar systems, it is recommended to implement a comprehensive monitoring and maintenance program. Regular inspections, performance evaluations, and necessary repairs or replacements should be conducted to control losses and maintain consistent energy generation and system efficiency.

7.2 Future Recommendations

Based on the findings and experience gained during this project, the following recommendations are provided for future action:

7.2.1 BIPV systems

Continued research and development efforts for new materials and technologies is essential to enhance the performance and aesthetics of BIPV systems. Focus should be given to enhancing the energy conversion efficiency of these modules and reducing their manufacturing costs, in order to create suitable and profitable elements to replace building construction materials and expand their applicability across various building types and designs, as well as urban settings.

An example of advancement in this industry, Solar Innova, a company based in Spain, has made significant strides in the development of a wide range of innovative building-integrated photovoltaic (BIPV) products. Their product selection includes colored BIPV tiles presented in figure 7.1, that can replace conventional building envelope materials, transforming them into active solar generators. These remarkable tiles present a breakthrough solution that seamlessly merges renewable energy generation with architectural aesthetics. The incorporation of Solar Innova's colored BIPV tiles aligns perfectly with the core objectives of this study, emphasizing the importance of early design considerations and the integration of renewable energy technologies.

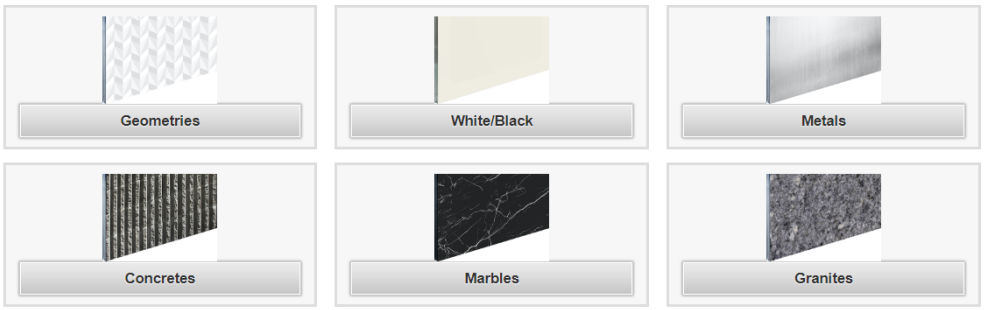

Figure 7.1 BIPV Colored tiles. [53]

Additionally, collaboration among industry stakeholders, including architects, engineers, manufacturers, and policymakers, is essential to establish common standards and guidelines for BIPV integration. Governments and regulatory bodies should introduce and update building codes and regulations to encourage the widespread adoption and incentive programs such as feed-in tariffs, tax credits, and grants can provide financial support and promote the adoption of BIPV systems.

7.2.2 Early Design Considerations for PV Integration in Building Construction

Integrating photovoltaic systems into building designs during the early construction phase offers numerous benefits. By considering PV integration at the initial stages of building design, architects, engineers, and developers can optimize energy generation, reduce environmental impact, enhance the building's sustainability credentials, and potentially lead to long-term cost savings. This paves the way for more efficient and environmentally friendly buildings in the future through the following means:

-Analyzing the building site's orientation and conducting shading studies that are essential to identify the optimal locations for PV panel installation. This early consideration ensures maximum solar exposure and minimizes the impact of shading from surrounding structures or natural features.

-Early consideration allows for proper reinforcement and integration of mounting systems as well as electrical infrastructure establishment which includes considerations such as adequate space for inverters, electrical panels, and proper wiring routes. This ensures safe and secure installations and eliminates the need for costly retrofitting and extensive electrical and structural modifications later on.

-Considering the aesthetic aspects of PV integration early in the design phase also ensures seamless integration with the building's architecture. Architects can incorporate PV panels into facades, canopies, or other design elements, creating an aesthetically pleasing and visually appealing outcome. This approach avoids the addition of PV systems as an afterthought, preserving the building's original design intent.

-Conducting an energy load analysis during the early design phase helps optimize the sizing and capacity of the PV system. By understanding the building's energy demand, designers can accurately determine the required PV capacity to offset a significant portion of the energy consumption which leads to reduced reliance on the grid.

7.2.3 Steps towards building decarbonization

As we look ahead to the future, it is crucial to expand our exploration of renewable energy sources beyond BIPV and wind systems to effectively decarbonize buildings and reduce their dependence on the grid.

One avenue to explore is the utilization of PV-T (Photovoltaic-Thermal) solar systems (Figure 7.2), which offer higher efficiency with the dual advantage of generating electricity and capturing thermal energy for various heating purposes. Moreover, other renewable energy sources such as geothermal systems (Figure 7.3), tap into the Earth's natural heat to provide heating and cooling solutions for buildings. By harnessing the stable and sustainable thermal energy beneath the Earth's surface, geothermal systems can significantly reduce a building's reliance on traditional heating and cooling methods, thereby contributing to decarbonization efforts.

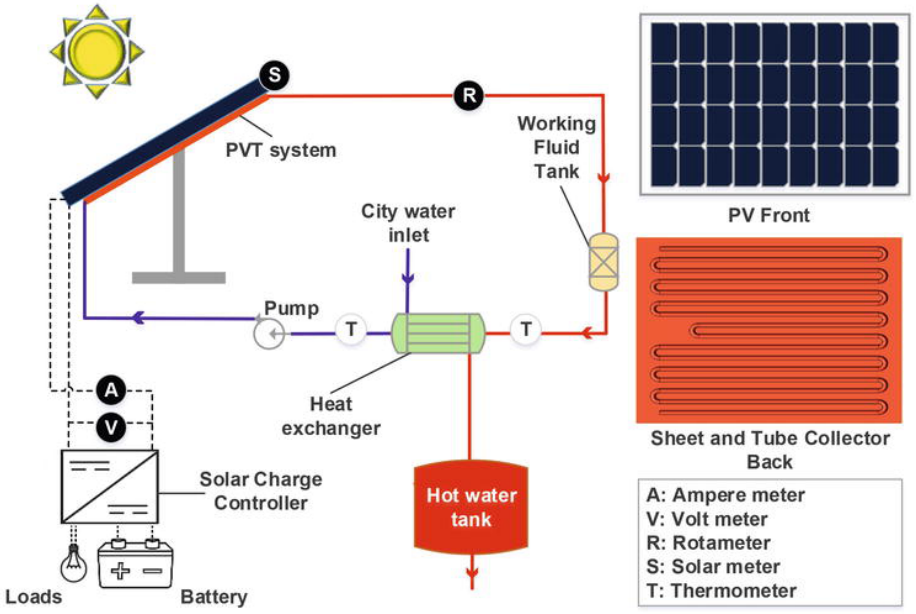

Figure 7.2 Solar photovoltaic-thermal collectors schematic. [54]

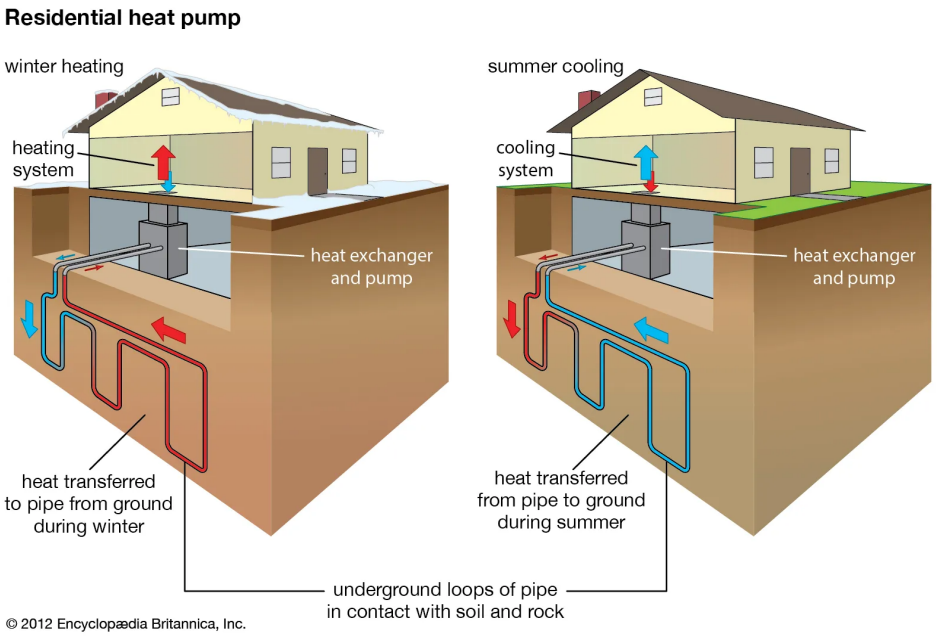

Figure 7.3 Geothermal systems for heating and cooling. [55]

In addition to exploring various renewable energy sources, it is crucial to emphasize the implementation of energy-saving measures within buildings, such as efficient equipment like lighting systems, smart thermostats, and improved insulation, which can significantly reduce overall energy consumption and further decrease reliance on the grid.

In conclusion, the successful integration of photovoltaic systems in building designs showcased in this study highlights the importance of pursuing similar projects on a larger scale. If multiple buildings across cities or urban areas were to adopt such sustainable practices and achieve comparable results, the cumulative impact would be significant. Not only would it contribute to a substantial reduction in carbon emissions and energy consumption, but it would also promote grid decentralization. Building integrated systems can generate electricity at the point of consumption, reducing the need for long-distance transmission of energy. This promotes grid independence and reduces the strain on it, especially during peak demand periods, and decreases the need for extensive grid infrastructure investments.

8. Bibliography

[1] European Commission, “A European Green Deal,” European Commission, 2019. https://ec.europa.eu/info/strategy/priorities-2019-2024/european-green-deal_en

[2] European Commission, “Energy efficient buildings,” Energy - European Commission, Jan. 06, 2020. https://ec.europa.eu/energy/en/topics/energy-efficiency/buildings

[3] European Commission, “Energy performance of buildings directive,” energy.ec.europa.eu, 2018.https://energy.ec.europa.eu/topics/energy-efficiency/energy-efficient-buildings/energy-performance-buildings-directive_en

[4] Ajuntament de Barcelona, “Barcelona for Climate | Ajuntament de Barcelona,” www.barcelona.cat. https://www.barcelona.cat/barcelona-pel-clima/en

[5]D. S. Pillai, V. Shabunko, and A. Krishna, “A comprehensive review on building integrated photovoltaic systems: Emphasis to technological advancements, outdoor testing, and predictive maintenance,” Renewable and Sustainable Energy Reviews, vol. 156, p. 111946, Mar. 2022, doi: https://doi.org/10.1016/j.rser.2021.111946.

[6] S. Pantic, L. Candanedo, and A. K. Athienitis, “Modeling of energy performance of a house with three configurations of building-integrated photovoltaic/thermal systems,” Energy and Buildings, vol. 42, no. 10, pp. 1779–1789, Oct. 2010, doi: https://doi.org/10.1016/j.enbuild.2010.05.014

[7] A Luque and S. Hegedus, Handbook of photovoltaic science and engineering. Chichester, West Sussex, U.K.: Wiley, 2011.

[8] V. M. Fthenakis and H. C. Kim, “Photovoltaics: Life-cycle analyses,” Solar Energy, vol. 85, no. 8, pp. 1609–1628, Aug. 2011, doi: https://doi.org/10.1016/j.solener.2009.10.002.

[9] M. A. Green, E. D. Dunlop, D. H. Levi, J. Hohl-Ebinger, M. Yoshita, and A. W. Y. Ho-Baillie, “Solar cell efficiency tables (version 54),” Progress in Photovoltaics: Research and Applications, vol. 27, no. 7, pp. 565–575, Jun. 2019, doi: https://doi.org/10.1002/pip.3171.

[10] International Renewable Energy Agency IRENA, Renewable power generation costs in 2018. International Renewable Energy Agency (IRENA), 2019 https://www.irena.org/-/media/Files/IRENA/Agency/Publication/2019/May/IRENA_Renewable-Power-Generations-Costs-in-2018.pdf?rev=7a3b6ab611bd41ab9ec399d2e70eaa31

[11] H. J. Snaith, "Present status and future prospects of perovskite photovoltaics," Nature Materials, vol. 17, no. 5, pp. 372–376, Apr. 2018, doi: https://doi.org/10.1038/s41563-018-0071-z.

[12] International Renewable Energy Agency IRENA, "Evolution of solar PV module cost by data source, 1970-2020 – Charts – Data & Statistics," IEA, Oct. 26, 2022. https://www.iea.org/data-and-https://www.iea.org/data-and-statistics/charts/evolution-of-solar-pv-module-cost-by-data-source-1970-2020

[13] A. Han, "Efficiency of solar PV, then, now and future – Solar photovoltaic," Lafayette.edu, Dec. 09, 2014. https://sites.lafayette.edu/egrs352-sp14-pv/technology/history-of-pv-technology/

[14] M. A. Green, Third Generation Photovoltaics. Springer Science & Business Media, 2006.

[15] Y.-J. Lee, B.-S. Kim, S. M. Ifitiquar, C. Park, and J. Yi, "Silicon solar cells: Past, present and the future," vol. 65, no. 3, pp. 355–361, Aug. 2014, doi: https://doi.org/10.3938/jkps.65.355.

[16] J. Marsh, "Monocrystalline vs. Polycrystalline Solar Panels | EnergySage," Solar News, Apr. 10, 2021. https://news.energysage.com/monocrystalline-vs-polycrystalline-solar/

[17] Soteris Kalogirou, *Solar energy engineering : processes and systems*. Burlington, Ma: Elsevier/Academic Press, 2009.

[18] S. Hong and J. Lee, "Recent Advances and Challenges toward Efficient Perovskite/Organic Integrated Solar Cells," vol. 16, no. 1, pp. 266–266, Dec. 2022, doi: https://doi.org/10.3390/en16010266.

[19] M. A. Green, "Solar cells—Operating principles, Technology and System Applications," Solar Energy, vol. 28, no. 5, p. 447, 1982, doi: https://doi.org/10.1016/0038-092x(82)90265-1.

[20] P. Jackson et al., "New world record efficiency for Cu(In,Ga)Se2 thin-film solar cells beyond 20%," Progress in Photovoltaics: Research and Applications, vol. 19, no. 7, pp. 894–897, Jan. 2011, doi: https://doi.org/10.1002/pip.1078.

[21] National Renewable Energy Laboratory (NREL), "Polycrystalline Thin-Film Photovoltaics," www.nrel.gov, 2022. https://www.nrel.gov/pv/polycrystalline-thin-film-photovoltaics.html

[22] P. Gipe, Wind energy basics : a guide to small and micro wind systems. White River Junction, Vt.: Chelsea Green Pub. Co, 1999.

[23] M. Bošnjaković, M. Katinić, R. Santa, and D. Marić, "Wind Turbine Technology Trends," Applied Sciences, vol. 12, no. 17, p. 8653, Aug. 2022, doi: https://doi.org/10.3390/app12178653.

[24] Z. Zhang, "Performance optimization of wind turbines," 2012, doi: https://doi.org/10.17077/etd.2wjjp4la.

[25] M. Islam, S. Mekhilef, and M. Hasan, "Single phase transformerless inverter topologies for grid-tied photovoltaic system: A review," Renewable and Sustainable Energy Reviews, vol. 45, pp. 69–86, May 2015, doi: https://doi.org/10.1016/j.rser.2015.01.009.

[26] D. Verma, S. Nema, R. Agrawal, Y. Sawle, and A. Kumar, "A Different Approach for Maximum Power Point Tracking (MPPT) Using Impedance Matching through Non-Isolated DC-DC Converters in Solar Photovoltaic Systems," Electronics, vol. 11, no. 7, p. 1053, Mar. 2022, doi: https://doi.org/10.3390/electronics11071053.

[27] I. Worighi, A. Maach, A. Hafid, O. Hegazy, and J. Van Mierlo, "Integrating renewable energy in smart grid system: Architecture, virtualization and analysis," Sustainable Energy, Grids and Networks, vol. 18, p. 100226, Jun. 2019, doi: https://doi.org/10.1016/j.segan.2019.100226.

[28] M. Y. Ali Khan, H. Liu, Z. Yang, and X. Yuan, "A Comprehensive Review on Grid Connected Photovoltaic Inverters, Their Modulation Techniques, and Control Strategies," Energies, vol. 13, no. 16, p. 4185, Aug. 2020, doi: https://doi.org/10.3390/en13164185.

[29] M. E. Ya'acob, H. Hizam, T. Khatib, and M. A. M. Radzi, "A Comparative Study of Three Types of Grid Connected Photovoltaic Systems Based on Actual Performance," Energy Conversion and Management, vol. 78, pp. 8–13, Feb. 2014, doi: https://doi.org/10.1016/j.enconman.2013.10.064.

[30] H. Lund, Renewable Energy Systems. Academic Press, 2014.

[31] G. Stapleton and S. Neill, Grid-Connected Solar Electric Systems. Hoboken: Taylor and Francis, 2012.

[32] International Renewable Energy Agency IRENA, "There's more to buildings than meets the eye: They hold a key to net zero emissions – Analysis," IEA, Feb. 15, 2023. https://www.iea.org/commentaries/there-s-more-to-buildings-than-meets-the-eye-they-hold-a-key-to-net-zero-emissions

[33] International Renewable Energy Agency IRENA, "Solar PV and wind supply about 40% of building electricity use by 2030 – Analysis," IEA, 2022. https://www.iea.org/reports/solar-pv-and-wind-supply-about-40-of-building-electricity-use-by-2030

[34] International Energy Agency Photovoltaic Power Systems Programme, "International Definitions of 'BIPV,'" Aug. 2018. Available: https://iea-pvps.org/wp-content/uploads/2020/02/IEA-PVPS_Task_15_Report_C0_International_definitions_of_BIPV_hrw_180823.pdf

[35] H. Joshi, "Building Integrated Photovoltaics: Pros, Cons & Cost in 2022," Solarfunda, Apr. 25, 2022. https://solarfunda.com/building-integrated-photovoltaics/

[36] UNEP Copenhagen Climate Centre (UNEP-CCC), "Building-integrated Wind Turbines | Climate Technology Centre & Network," www.ctc-n.org. https://www.ctc-n.org/technologies/building-integrated-wind-turbines

[37]J. Park, H.-J. Jung, S.-W. Lee, and J. Park, "A New Building-Integrated Wind Turbine System Utilizing the Building," Energies, vol. 8, no. 10, pp. 11846–11870, Oct. 2015, doi: https://doi.org/10.3390/en81011846.

[38] Ajuntament de Barcelona, "Polítiques energètiques de l'Ajuntament | Energia Barcelona | Ajuntament de Barcelona," www.energia.barcelona. https://www.energia.barcelona/ca/politiques-energetiques-de-lajuntament

[39] Ajuntament de Barcelona, "Ajuts I Bonificacions | Energia Barcelona | Ajuntament De Barcelona," www.energia.barcelona. https://www.energia.barcelona/ca/ajuts-i-bonificacions

[40] Ajuntament de Barcelona, "Generar Energia | Energia Barcelona | Ajuntament De Barcelona," www.energia.barcelona. https://www.energia.barcelona/ca/generar-energia

[41] Ajuntament de Barcelona, "Map: How Much Energy Can You generate? | Energia Barcelona | Barcelona City Council," www.energia.barcelona. https://www.energia.barcelona/en/map-how-much-energy-can-you-generate

[42]National Renewable Energy Center (CENER), "Mapa Eólico Ibérico," www.mapaeolicoiberico.com. https://www.mapaeolicoiberico.com/map

[43] Vortex Factoria De Calculs, "Vortex Factoria De Calculs, S.L. - Log in to Vortex Interface," api.vortexfdc.com. https://interface.vortexfdc.com

[44] SIRENA Platform. (n.d.). Retrieved from https://upcsirena.app.dexma.com/I_189529/analysis/consumption/display.htm

[45]Climate Data, “Barcelona climate: Average Temperature, Weather by month, Barcelona Water Temperature - Climate-Data.org,” en.climate-data.org. https://en.climate-data.org/europe/spain/catalonia/barcelona-1564/

[46] Wind Turbine Star, “Roof Mount Tower for Wind Turbine – Aeolos Roof Top Tower for Vertical Wind Turbines, Roof Mounted Towers,” www.windturbinestar.com. https://www.windturbinestar.com/roof-mount-tower.htmll

[47]M. D’Orazio, C. Di Perna, and E. Di Giuseppe, “Performance Assessment of Different Roof Integrated Photovoltaic Modules under Mediterranean Climate,” Energy Procedia, vol. 42, pp. 183–192, 2013, doi: https://doi.org/10.1016/j.egypro.2013.11.018.

[48] Windy Nation, “Choosing the Right Wire Size,” Windy Nation Inc, Feb. 25, 2023. https://www.windynation.com/blogs/articles/choosing-the-right-wire-size

[49] Kingsmill Industries, “USA to European Cable Size Chart,” Kingsmill Industries. https://kingsmillindustries.com/product-guide/usa-to-european-cable-size-chart/

[50] Oficina Catalana Del Canvi Climatic, “Guia De Càlcul d’emissions De Gasos Amb Efecte d’hivernacle (GEH) 11 De Maig De 2023,” May 2023. Accessed: Jun. 05, 2023. [Online]. Available: https://canviclimatic.gencat.cat/web/.content/04_ACTUA/Com_calcular_emissions_GEH/guia_de_calcul_demissions_de_co2/2023_Guia-de-calcul-emissions-GEH.pdf

[51] Universitat Politècnica De Catalunya , “Consum I Despesa d’energia a La UPC,” Comunitat UPC Sostenible. https://sostenible.upc.edu/ca/energia/emergencia-energetica/evolucio-del-consum-denergia-a-la-upc

[52] The Engineering Toolbox, “Copper and Aluminum Wire - Electrical Resistance,” www.engineeringtoolbox.com. https://www.engineeringtoolbox.com/copper-aluminum-conductor-resistance-d_1877.html

[53] Solar Innova, “Colored BIPV Product Selection,” solarinnova.net. https://solarinnova.net/en/products/photovoltaic/modules/bipv/colored

[54] A. Farzanehnia and M. Sardarabadi, “Exergy in Photovoltaic/Thermal Nanofluid-Based Collector Systems,” www.intechopen.com, Oct. 23, 2019. https://www.intechopen.com/chapters/66854

[55] J. W. Lund, “Geothermal Energy,” Encyclopædia Britannica. Apr. 30, 2018. Available: https://www.britannica.com/science/geothermal-energy

Annex A

A1. Product Datasheets

In the annex section of this thesis, a collection of datasheets pertaining to the various components and systems discussed throughout the study are presented. These data sheets provide detailed technical information, specifications, and performance data related to the equipment and technologies.

A1.1 High Roof

Solar module: Jinko Solar JKM580N-72HL4-BDV

LINEAR PERFORMANCE WARRANTY

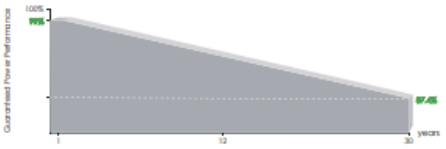

12 Year Product Warranty

30 Year Linear Power Warranty

0.40% Annual Degradation Over 30 years

Engineering Drawings

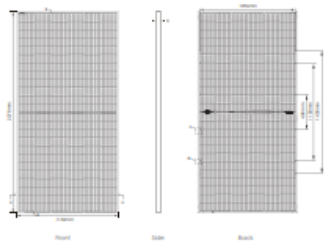

Packaging Configuration

(Two pallets = One stack)

36pcs/pallets, 72pcs/stack, 720pcs/ 40'HQ Container

Electrical Performance & Temperature Dependence

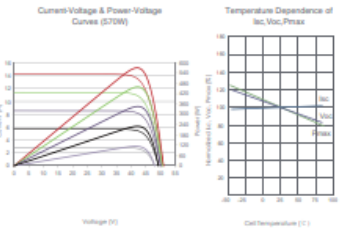

Mechanical Characteristics

Cell Type	N type Mono-crystalline
No. of cells	144 (2×72)
Dimensions	2278×1134×30mm (89.69×44.65×1.18 inch)
Weight	32 kg (70.55 lbs)
Front Glass	2.0mm, Anti-Reflection Coating
Back Glass	2.0mm, Heat Strengthened Glass
Frame	Anodized Aluminium Alloy
Junction Box	IP68 Rated
Output Cables	TUV 1×4.0mm (+): 400mm , (-): 200mm or Customized Length

SPECIFICATIONS

Module Type	JKM560N-72HL4-BDV		JKM565N-72HL4-BDV		JKM570N-72HL4-BDV		JKM575N-72HL4-BDV		JKM580N-72HL4-BDV	
	STC	NOCT	STC	NOCT	STC	NOCT	STC	NOCT	STC	NOCT
Maximum Power (Pmax)	560Wp	421Wp	565Wp	425Wp	570Wp	429Wp	575Wp	432Wp	580Wp	436Wp
Maximum Power Voltage (Vmp)	41.95V	39.39V	42.14V	39.52V	42.29V	39.65V	42.44V	39.78V	42.59V	39.87V
Maximum Power Current (Imp)	13.35A	10.69A	13.41A	10.75A	13.48A	10.81A	13.55A	10.87A	13.62A	10.94A
Open-circuit Voltage (Voc)	50.67V	48.13V	50.87V	48.32V	51.07V	48.51V	51.27V	48.70V	51.47V	48.89V
Short-circuit Current (Isc)	14.13A	11.41A	14.19A	11.46A	14.25A	11.50A	14.31A	11.55A	14.37A	11.60A
Module Efficiency STC (%)	21.68%		21.87%		22.07%		22.26%		22.45%	
Operating Temperature(°C)	-40°C~+85°C									
Maximum system voltage	1500VDC (IEC)									
Maximum series fuse rating	30A									
Power tolerance	0~+3%									
Temperature coefficients of Pmax	-0.29%/°C									
Temperature coefficients of Voc	-0.25%/°C									
Temperature coefficients of Isc	0.045%/°C									
Nominal operating cell temperature (NOCT)	45±2°C									
Refer. Bifacial Factor	80±5%									

BIFACIAL OUTPUT-REARSIDE POWER GAIN

5%	Maximum Power (Pmax)	588Wp	593Wp	599Wp	604Wp	609Wp
	Module Efficiency STC (%)	22.76%	22.97%	23.17%	23.37%	23.57%
15%	Maximum Power (Pmax)	644Wp	650Wp	656Wp	661Wp	667Wp
	Module Efficiency STC (%)	24.93%	25.15%	25.37%	25.60%	25.82%
25%	Maximum Power (Pmax)	700Wp	706Wp	713Wp	719Wp	725Wp
	Module Efficiency STC (%)	27.10%	27.34%	27.58%	27.82%	28.07%

STC: Irradiance 1000W/m² | Cell Temperature 25°C | AM=1.5

NOCT: Irradiance 800W/m² | Ambient Temperature 20°C | AM=1.5 | Wind Speed 1m/s

JKM560-580N-72HL4-BDV-F4-EN

Inverter: Huawei- SUN2000-30KTL-M3

SUN2000-30/36/40KTL-M3

Smart PV Controller

HUAWEI

Smart
8 strings intelligent monitoring

Efficient
Max. efficiency 98.7%

Safe
Fuse free design

Reliable
Type II surge arresters for DC & AC

Efficiency Curve

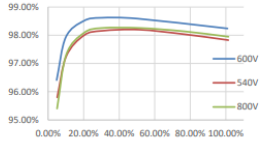

SUN2000-30/36/40KTL-M3

Circuit Diagram

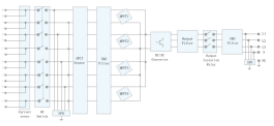

SOLAR.HUAWEI.COM

SUN2000-30/36/40KTL-M3

Technical Specification

Technical Specification	SUN2000-30KTL-M3	SUN2000-36KTL-M3	SUN2000-40KTL-M3
Efficiency			
Max. Efficiency	98.7%		
European Efficiency	98.4%		
Input			
Max. Input Voltage [1]	1,100 V		
Max. Current per MPPT	26 A		
Max. Short Circuit Current per MPPT	40 A		
Start Voltage	200 V		
MPPT Operating Voltage Range [2]	200 V ~ 1000 V		
Rated Input Voltage	600 V		
Number of Inputs	8		
Number of MPP Trackers	4		
Output			
Rated AC Active Power	30,000 W	36,000 W	40,000 W
Max. AC Apparent Power	33,000 VA	40,000 VA	44,000 VA
Rated Output Voltage	230 Vac / 400 Vac, 3W/N+PE		
Rated AC Grid Frequency	50 Hz / 60 Hz		
Rated Output Current	43.3 A	52.0 A	57.8 A
Max. Output Current	47.9 A	58.0 A	63.8 A
Adjustable Power Factor Range	0.8 LG ... 0.8 LD		
Max. Total Harmonic Distortion	< 3%		
Protection			
Input-side Disconnection Device	Yes		
Anti-islanding Protection	Yes		
AC Overcurrent Protection	Yes		
DC Reverse-polarity Protection	Yes		
PV-array String Fault Monitoring	Yes		
DC Surge Arrester	Yes		
AC Surge Arrester	Yes		
DC Insulation Resistance Detection	Yes		
Residual Current Monitoring Unit	Yes		
Arc Fault Protection	Yes		
Ripple Receiver Control	Yes		
Integrated PID Recovery [3]	Yes		
Communication			
Display	LED Indicators, Integrated WLAN + FusionSolar APP		
RS485	Yes		
Smart Dongle	WLAN/Ethernet via Smart Dongle-WLAN-FE (Optional) 4G / 3G / 2G via Smart Dongle-4G (Optional)		
Monitoring BUS (MBUS)	Yes (Isolation Transformer required)		

A1.2 Facade 1- A & B

Solar module: Jinko Solar JKM585N-72HL4-V

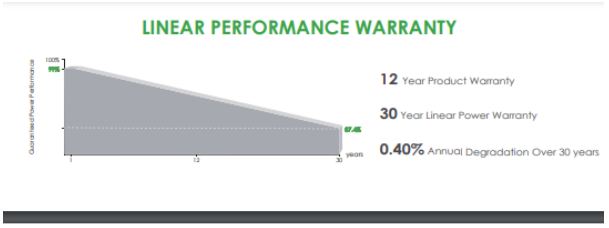

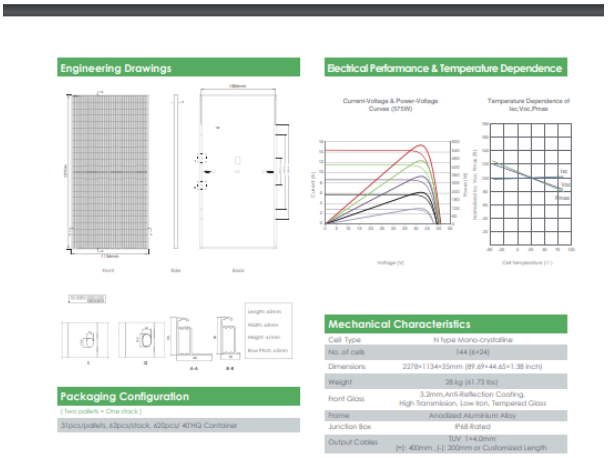

SPECIFICATIONS

Module Type	JKM565N-72HL4 JKM565N-72HL4-V		JKM570N-72HL4 JKM570N-72HL4-V		JKM575N-72HL4 JKM575N-72HL4-V		JKM580N-72HL4 JKM580N-72HL4-V		JKM585N-72HL4 JKM585N-72HL4-V	
	STC	NOCT	STC	NOCT	STC	NOCT	STC	NOCT	STC	NOCT
Maximum Power (Pmax)	565Wp	425Wp	570Wp	429Wp	575Wp	432Wp	580Wp	436Wp	585Wp	440Wp
Maximum Power Voltage (Vmp)	41.92V	39.38V	42.07V	39.51V	42.22V	39.60V	42.37V	39.69V	42.52V	39.81V
Maximum Power Current (Imp)	13.48A	10.79A	13.55A	10.85A	13.62A	10.92A	13.69A	10.99A	13.76A	11.05A
Open-circuit Voltage (Voc)	50.60V	48.06V	50.74V	48.20V	50.88V	48.33V	51.02V	48.46V	51.16V	48.60V
Short-circuit Current (Isc)	14.23A	11.49A	14.31A	11.55A	14.39A	11.62A	14.47A	11.68A	14.55A	11.75A
Module Efficiency STC (%)	21.87%		22.07%		22.26%		22.45%		22.65%	
Operating Temperature(℃)	-40℃~+85℃									
Maximum system voltage	1000/1500VDC (IEC)									
Maximum series fuse rating	25A									
Power tolerance	0~+3%									
Temperature coefficients of Pmax	-0.29%/℃									
Temperature coefficients of Voc	-0.25%/℃									
Temperature coefficients of Isc	0.045%/℃									
Nominal operating cell temperature (NOCT)	45±2℃									

*STC: Irradiance 1000W/m² Cell Temperature 25℃ AM=1.5
NOCT: Irradiance 800W/m² Ambient Temperature 20℃ AM=1.5 Wind Speed 1m/s

JKM565-585N-72HL4-(V)-F3-EN

Inverter (Facade 1-A): Solax X3-PRO G2-25

X3-PRO G2

8.0kW/10.0kW/12.0kW/15.0kW
17.0kW/20.0kW/25.0kW/30.0kW

Features

High-efficiency
- Maximum efficiency is up to 98.5%
- Low startup voltage, ultrawide MPPT voltage range
- 150% DC oversizing, 110% AC overloading output
- In-built global MPP scan for higher yield efficiency

Safe
- SPD type II protection on both AC&DC
- ARC protection (Optional)
- IP66 protection

Smart
- Built-in export power control
- Intelligent load management - heat pump (Adapter Box required)
- 24h monitoring and maintenance (Optional)
- Multiple monitoring methods, Pocket WiFi/LAN (Optional)/4G (Optional)

Economic
- Ultra-high power density
- Maximum 32A DC input current per MPP tracker, support high power solar panels
- Up to 3 MPPTs, 2 strings per MPPT
- Support Master/Slave parallel function

SOLAX POWER

X3-PRO G2

	X3-PRO-8K-G2	X3-PRO-10K-G2	X3-PRO-12K-G2	X3-PRO-15K-G2	X3-PRO-17K-G2	X3-PRO-20K-G2	X3-PRO-25K-G2	X3-PRO-30K-G2
DC INPUT								
Max. PV array input power [Wp]	12000	15000	18000	22500	25500	30000	37500	45000
Max. PV input voltage [V]	1100	1100	1100	1100	1100	1100	1100	1100
Start startup voltage [V]	200	200	200	200	200	200	200	200
Nominal input voltage [V]	650	650	650	650	650	650	650	650
MPP tracker voltage range [V]	160~980							
No. of MPP trackers	2	2	2	2	2	2	3	3
Strings per MPP tracker	2	2	2	2	2	2	2	2
Max. input current per MPPT [A]	32/32	32/32	32/32	32/32	32/32	32/32	32/32/32	32/32/32
Max. short circuit current per MPPT [A]	40/40	40/40	40/40	40/40	40/40	40/40	40/40/40	40/40/40
AC OUTPUT								
Nominal AC output power [W]	8000	10000	12000	15000	17000	20000	25000	30000
Nominal AC output current [A]	12.2/11.6	15.2/14.5	18.2/17.4	22.8/21.8	25.8/24.7	30.3/29	37.9/36.3	45.5/43.5
Max. AC output apparent power [VA]	8800	11000	13200	16500	18700	22000	27500	33000
Max. AC output current [A]	13.2	16	19.3	24.2	27.5	33.6	41.8	45.5
Nominal AC voltage [V]	220/380, 230/400, 3/N/PE, 3/PE							
Nominal grid frequency [Hz]	50/60							
Displacement power factor	0.8 leading ~ 0.8 lagging							
THDi (Rated power) [%]	<3							

SYSTEM DATA								
Max. efficiency [%]	98.20	98.20	98.20	98.30	98.30	98.30	98.50	98.50
Euro efficiency [%]	97.70	97.70	97.70	97.80	97.80	97.80	98.00	98.00
Standby consumption(Night) [W]	<3							
Ingress protection	IP66							
Operating temperature range [°C]	-30~+60 (Derating above 45)							
Max. operation altitude [m]	4000 (Derating above 3000)							
Relative humidity [%]	0~100							
Typical noise emission [dB]	<35	<35	<35	<55	<55	<55	<55	<58
Storage temperature [°C]	-30~+60							
Dimensions (WxHxD) [mm]	482x417x181							
Weight [kg]	24.5			26			28	
Cooling concept	Natural cooling			Smart fan cooling				
Communication interfaces	USB / RS485 / DRM / Pocket WiFi (Optional: Pocket LAN/4G) / Adapter box (Optional)							
PROTECTION								
Over/under voltage protection	YES							
DC isolation protection	YES							
Grid monitoring	YES							
DC injection monitoring	YES							
Residual current detection	YES							
Anti-islanding protection	YES							
Over Temp protection	YES							
SPD (DC/AC)	Type II / Type II							
AC auxiliary power supply (APS)	Optional							
Arc-fault circuit interrupter (AFCI)	Optional							
STANDARD								
Safety	IEC/EN 62109-1; IEC/EN 62109-2; NB/T 32004							
EMC	IEC/EN 61000; NB/T 32004							
Certification	VDE4105; EN 50549; AS 4777.2; VDE4105; IEC 61727; IEC 62116; IEC 61683; IEC 60068; EN 50530; NB/T 32004							

*V2.2. Information may be subject to modify without notice. 650.00004.00

Inverter (Facade 1-B): Huawei- SUN2000-36KTL-M3

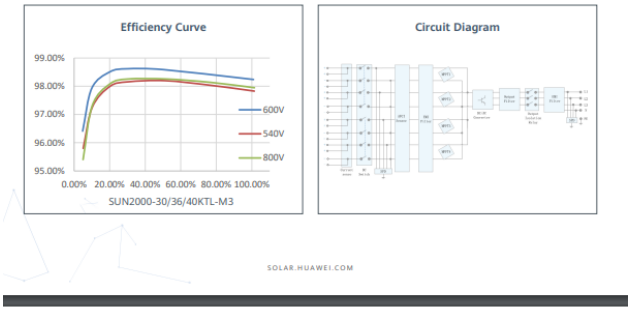

SUN2000-30/36/40KTL-M3

Technical Specification

Technical Specification	SUN2000-30KTL-M3	SUN2000-36KTL-M3	SUN2000-40KTL-M3
Efficiency			
Max. Efficiency	98.7%		
European Efficiency	98.4%		
Input			
Max. Input Voltage [1]	1,100 V		
Max. Current per MPPT	26 A		
Max. Short Circuit Current per MPPT	40 A		
Start Voltage	200 V		
MPPT Operating Voltage Range [2]	200 V ~ 1000 V		
Rated Input Voltage	600 V		
Number of Inputs	8		
Number of MPP Trackers	4		
Output			
Rated AC Active Power	30,000 W	36,000 W	40,000 W
Max. AC Apparent Power	33,000 VA	40,000 VA	44,000 VA
Rated Output Voltage	230 Vac / 400 Vac, 3W/N+PE		
Rated AC Grid Frequency	50 Hz / 60 Hz		
Rated Output Current	43.3 A	52.0 A	57.8 A
Max. Output Current	47.9 A	58.0 A	63.8 A
Adjustable Power Factor Range	0.8 LG ... 0.8 LD		
Max. Total Harmonic Distortion	< 3%		
Protection			
Input-side Disconnection Device	Yes		
Anti-islanding Protection	Yes		
AC Overcurrent Protection	Yes		
DC Reverse-polarity Protection	Yes		
PV-array String Fault Monitoring	Yes		
DC Surge Arrester	Yes		
AC Surge Arrester	Yes		
DC Insulation Resistance Detection	Yes		
Residual Current Monitoring Unit	Yes		
Arc Fault Protection	Yes		
Ripple Receiver Control	Yes		
Integrated PID Recovery [3]	Yes		
Communication			
Display	LED Indicators, Integrated WLAN + FusionSolar APP		
RS485	Yes		
Smart Dongle	WLAN/Ethernet via Smart Dongle-WLAN-FE (Optional) 4G / 3G / 2G via Smart Dongle-4G (Optional)		
Monitoring BUS (MBUS)	Yes (Isolation Transformer required)		

A1.3 Facade 2

Solar module: Jinko Solar JKM630N-78HL4

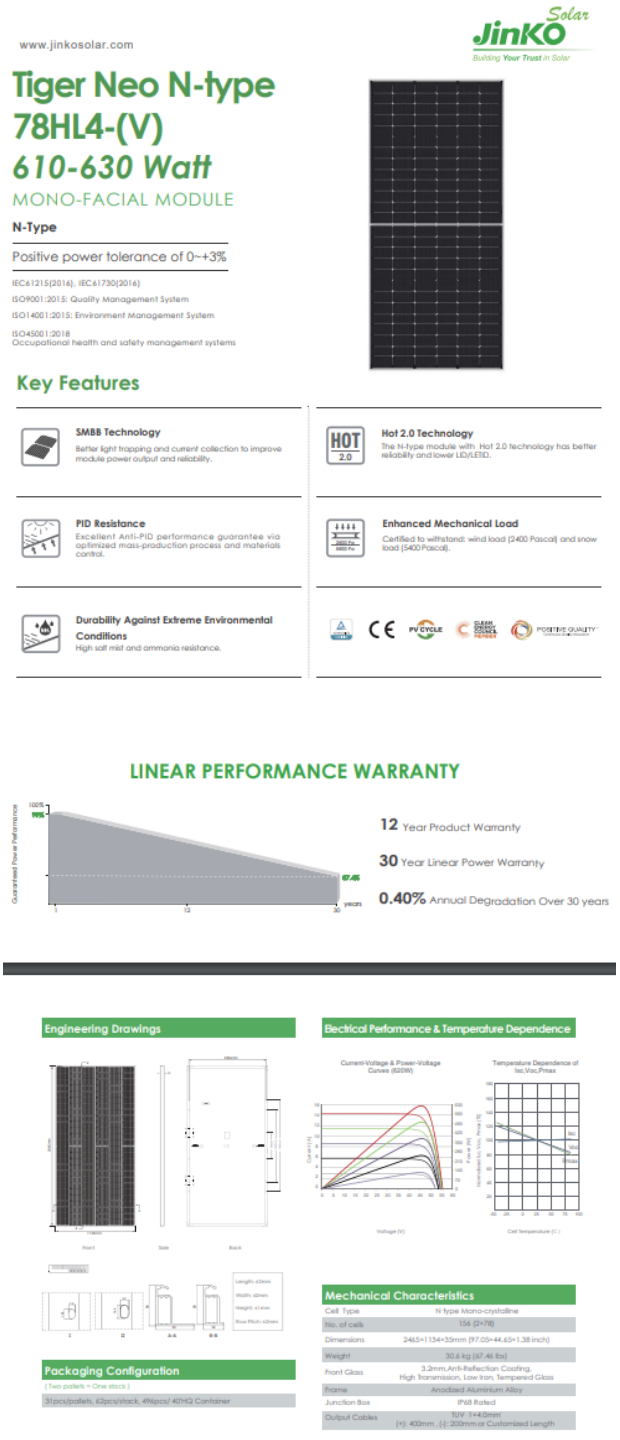

www.jinkosolar.com

Tiger Neo N-type 78HL4-(V)

610-630 Watt

MONO-FACIAL MODULE

N-Type

Positive power tolerance of 0~+3%

IEC61215(2016), IEC61730(2016)

ISO9001:2015: Quality Management System

ISO14001:2015: Environment Management System

ISO45001:2018 Occupational health and safety management systems

Key Features

SMBB Technology

Better light trapping and current collection to improve module power output and reliability.

Hot 2.0 Technology

The N-type module with Hot 2.0 technology has better reliability and lower LID/LETID.

PID Resistance

Excellent Anti-PID performance guarantee via optimized mass-production process and materials control.

Enhanced Mechanical Load

Certified to withstand: wind load (2400 Pascal) and snow load (5400 Pascal).

Durability Against Extreme Environmental Conditions

High salt mist and ammonia resistance.

LINEAR PERFORMANCE WARRANTY

12 Year Product Warranty

30 Year Linear Power Warranty

0.40% Annual Degradation Over 30 years

Engineering Drawings

Electrical Performance & Temperature Dependence

Mechanical Characteristics

Cell Type	N-type Mono-crystalline
No. of cells	156 (2×78)
Dimensions	2465×1134×35mm (97.05×44.65×1.38 inch)
Weight	30.6 kg (67.46 lbs)
Front Glass	3.2mm,Anti-Reflection Coating, High Transmission, Low Iron, Tempered Glass
Frame	Anodized Aluminium Alloy
Junction Box	IP68 Rated
Output Cables	TUV 1×4.0mm² (+): 400mm, (-): 200mm or Customized Length

Packaging Configuration

(Two pallets = One stack)

31pcs/pallet, 62pcs/stack, 496pcs/ 40HQ Container

SPECIFICATIONS

Module Type	JKM610N-78HL4 JKM610N-78HL4-V		JKM615N-78HL4 JKM615N-78HL4-V		JKM620N-78HL4 JKM620N-78HL4-V		JKM625N-78HL4 JKM625N-78HL4-V		JKM630N-78HL4 JKM630N-78HL4-V	
	STC	NOCT	STC	NOCT	STC	NOCT	STC	NOCT	STC	NOCT
Maximum Power (Pmax)	610Wp	459Wp	615Wp	462Wp	620Wp	466Wp	625Wp	470Wp	630Wp	474Wp
Maximum Power Voltage (Vmp)	45.59V	42.28V	45.69V	42.39V	45.79V	42.50V	45.92V	42.61V	46.02V	42.72V
Maximum Power Current (Imp)	13.38A	10.85A	13.46A	10.91A	13.54A	10.97A	13.61A	11.03A	13.69A	11.09A
Open-circuit Voltage (Voc)	55.25V	52.48V	55.40V	52.62V	55.55V	52.77V	55.70V	52.91V	55.85V	53.05V
Short-circuit Current (Isc)	14.11A	11.39A	14.18A	11.45A	14.25A	11.50A	14.32A	11.56A	14.39A	11.62A
Module Efficiency STC (%)	21.82%		22.00%		22.18%		22.36%		22.54%	
Operating Temperature(℃)	-40℃~+85℃									
Maximum system voltage	1000/1500VDC (IEC)									
Maximum series fuse rating	25A									
Power tolerance	0~+3%									
Temperature coefficients of Pmax	-0.29%/℃									
Temperature coefficients of Voc	-0.25%/℃									
Temperature coefficients of Isc	0.045%/℃									
Nominal operating cell temperature (NOCT)	45±2℃									

*STC: Irradiance 1000W/m² Cell Temperature 25°C AM=1.5

NOCT: Irradiance 800W/m² Ambient Temperature 20°C AM=1.5 Wind Speed 1m/s

JKM610-630N-78HL4-(V)-F3-EN

Inverter: Huawei SUN2000-60KTL-M0

Inversor de String Inteligente (SUN2000-60KTL-M0)

HUAWEI

Especificaciones técnicas	SUN2000-60KTL-M0
	Eficiencia
Eficiencia máxima	98.9% @480 Vac; 98.7% @380 Vac / 400 Vac
Eficiencia europea	98.7% @480 Vac; 98.5% @380 Vac / 400 Vac
	Entrada
Máx. tensión de entrada	1,100 V
Máx. intensidad por MPPT	22 A
Máx. intensidad de cortocircuito por MPPT	30 A
tensión de entrada inicial	200 V
Rango de tensión de operación de MPPT	200 V~1,000 V
tensión nominal de entrada	600 V @380 Vac / 400 Vac; 720 V @480 Vac
Máx. cantidad de entradas	12
Cantidad de MPPT	6
	Salida
Potencia nominal activa de CA	60,000 W
Máx. potencia aparente de CA	66,000 VA
Máx. potencia activa de CA (cosφ=1)	66,000 W
tensión nominal de salida	220V / 380V, 230V / 400V, default 3W+N+PE; 3W+PE optional in settings 277V / 480V, 3W+PE
Frecuencia nominal de red de CA	50 Hz / 60 Hz
intensidad de salida nominal	91.2 A @380 Vac, 86.7 A @400 Vac, 72.2 A @480 Vac
Máx. intensidad de salida	100 A @380 Vac, 95.3 A @400 Vac, 79.4 A @480 Vac
Factor de potencia ajustable	0.8 LG ... 0.8 LD
Máx. distorsión armónica total	< 3%
	Protección
Dispositivo de desconexión del lado de entrada	Sí
Protección contra funcionamiento en isla	Sí
Protección contra sobreintensidad de CA	Sí
Protección contra polaridad inversa de CC	Sí
monitorización de fallas en strings de sistemas fotovoltaicos	Sí
Protector contra sobreintensidad de CC	Tipo II
Protector contra sobreintensidad de CA	Tipo II
Detección de aislamiento de CC	Sí
Unidad de monitorización de la intensidad Residual	Sí
	Comunicación
Visualización	Indicadores LED, Bluetooth + APP
RS485	Sí
USB	Sí
Comunicación por línea de alimentación eléctrica (PLC)	Sí

	General
Dimensiones (ancho x altura x profundidad)	1,075 x 555 x 300 mm (42.3 x 21.9 x 11.8 pulgadas)
Peso (con soporte de montaje)	74 kg (163.1 lb.)
Rango de temperatura de operación	-25°C ~ 60°C (-13°F ~ 140°F)
Enfriamiento	Convección natural
Altitud de operación	4,000 m (13,123 ft.)
Humedad relativa	0 ~ 100%
Conector de CC	Amphenol Helios H4
Conector de CA	Terminal de PG resistente al agua + Arandela
Clase de protección	IP65
Topología	Sin transformador
	Cumplimiento de normas *(Más información disponible a pedido)*
Certificado	EN 62109-1/-2, IEC 62109-1/-2, EN 50530, IEC 62116, IEC 62910, IEC 60068, IEC 61683
Código de red	IEC 61727, VDE 4105/0126, UTE C 15-712-1, EN 50438, CLC/TS 50549-1, CEI 0-16/21, C10/11, RD 1699, PO 12.9

Curva de eficiencia

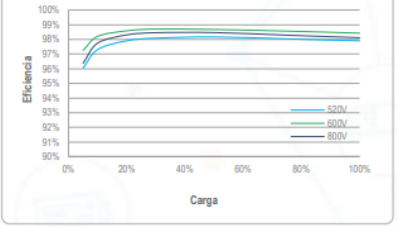

Esquema eléctrico

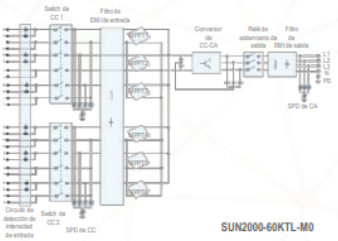

Always Available for Highest Yields

solar.huawei.com/es/

A1.4 Balcony Terrasse

Solar module: SolarInnova SI-ESF-M-BIPV-BL-RL-M156-4

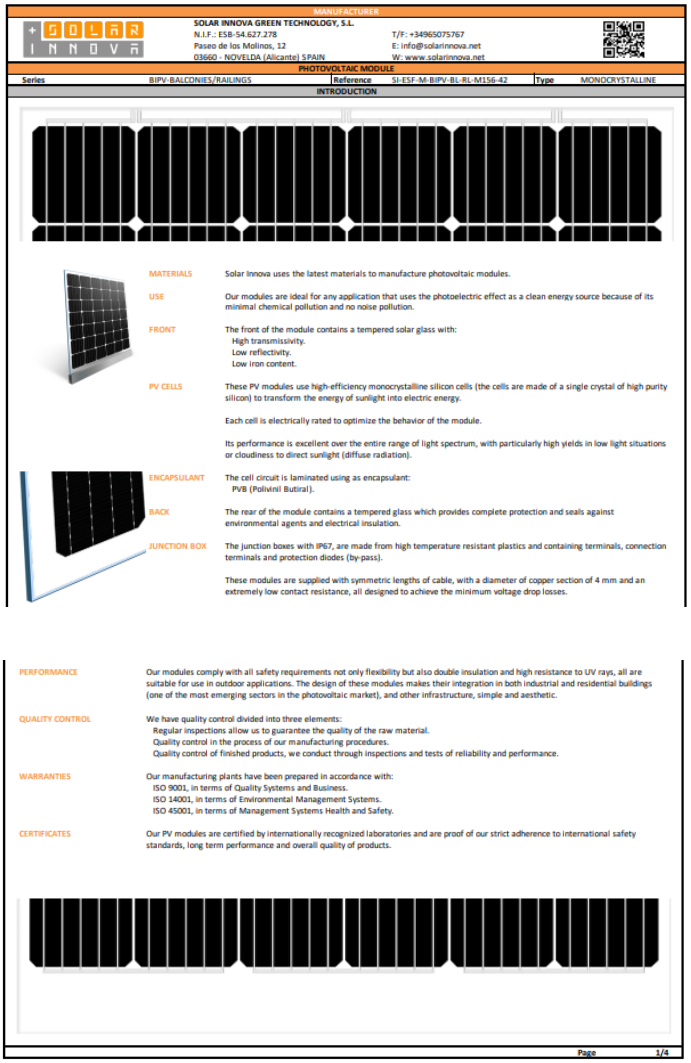

MANUFACTURER

SOLAR INNOVA GREEN TECHNOLOGY, S.L.
N.I.F.: ESB-54.627.278
Paseo de los Molinos, 12
03660 - NOVELDA (Alicante) SPAIN
T/F: +34965075767
E: info@solarinnova.net
W: www.solarinnova.net

PHOTOVOLTAIC MODULE

Series	BIPV-BALCONIES/RAILINGS	Reference	SI-ESF-M-BIPV-BL-RL-M156-42	Type	MONOCRYSTALLINE

INTRODUCTION

MATERIALS — Solar Innova uses the latest materials to manufacture photovoltaic modules.

USE — Our modules are ideal for any application that uses the photoelectric effect as a clean energy source because of its minimal chemical pollution and no noise pollution.

FRONT — The front of the module contains a tempered solar glass with:
- High transmissivity.
- Low reflectivity.
- Low iron content.

PV CELLS — These PV modules use high-efficiency monocrystalline silicon cells (the cells are made of a single crystal of high purity silicon) to transform the energy of sunlight into electric energy.

Each cell is electrically rated to optimize the behavior of the module.

Its performance is excellent over the entire range of light spectrum, with particularly high yields in low light situations or cloudiness to direct sunlight (diffuse radiation).

ENCAPSULANT — The cell circuit is laminated using as encapsulant:
- PVB (Polivinil Butiral).

BACK — The rear of the module contains a tempered glass which provides complete protection and seals against environmental agents and electrical insulation.

JUNCTION BOX — The junction boxes with IP67, are made from high temperature resistant plastics and containing terminals, connection terminals and protection diodes (by-pass).

These modules are supplied with symmetric lengths of cable, with a diameter of copper section of 4 mm and an extremely low contact resistance, all designed to achieve the minimum voltage drop losses.

PERFORMANCE — Our modules comply with all safety requirements not only flexibility but also double insulation and high resistance to UV rays, all are suitable for use in outdoor applications. The design of these modules makes their integration in both industrial and residential buildings (one of the most emerging sectors in the photovoltaic market), and other infrastructure, simple and aesthetic.

QUALITY CONTROL — We have quality control divided into three elements:
- Regular inspections allow us to guarantee the quality of the raw material.
- Quality control in the process of our manufacturing procedures.
- Quality control of finished products, we conduct through inspections and tests of reliability and performance.

WARRANTIES — Our manufacturing plants have been prepared in accordance with:
- ISO 9001, in terms of Quality Systems and Business.
- ISO 14001, in terms of Environmental Management Systems.
- ISO 45001, in terms of Management Systems Health and Safety.

CERTIFICATES — Our PV modules are certified by internationally recognized laboratories and are proof of our strict adherence to international safety standards, long term performance and overall quality of products.

Page 1/4

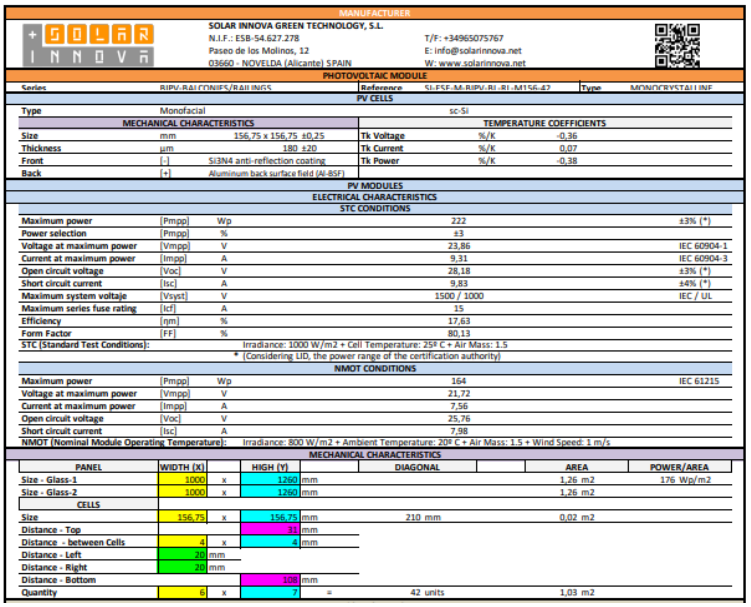

MANUFACTURER

SOLAR INNOVA GREEN TECHNOLOGY, S.L.
N.I.F.: ESB-54.627.278
Paseo de los Molinos, 12
03660 - NOVELDA (Alicante) SPAIN
T/F: +34965075767
E: info@solarinnova.net
W: www.solarinnova.net

PHOTOVOLTAIC MODULE

Series: RIPV-BALCONIES/RAILINGS | Reference: SI-FSF-M-RIPV-BI-BL-M156-42 | Type: MONOCRYSTALLINE

PV CELLS

Type	Monofacial			sc-Si	
MECHANICAL CHARACTERISTICS			**TEMPERATURE COEFFICIENTS**		
Size	mm	156,75 x 156,75 ±0,25	Tk Voltage	%/K	-0,36
Thickness	µm	180 ±20	Tk Current	%/K	0,07
Front	[-]	Si3N4 anti-reflection coating	Tk Power	%/K	-0,38
Back	[+]	Aluminium back surface field (Al-BSF)			

PV MODULES

ELECTRICAL CHARACTERISTICS

STC CONDITIONS

Maximum power	[Pmpp]	Wp	222	±3% (*)
Power selection	[Pmpp]	%	±3	
Voltage at maximum power	[Vmpp]	V	23,86	IEC 60904-1
Current at maximum power	[Impp]	A	9,31	IEC 60904-3
Open circuit voltage	[Voc]	V	28,18	±3% (*)
Short circuit current	[Isc]	A	9,83	±4% (*)
Maximum system voltaje	[Vsyst]	V	1500 / 1000	IEC / UL
Maximum series fuse rating	[Icf]	A	15	
Efficiency	[ηm]	%	17,63	
Form Factor	[FF]	%	80,13	

STC (Standard Test Conditions): Irradiance: 1000 W/m2 + Cell Temperature: 25º C + Air Mass: 1.5
* (Considering LID, the power range of the certification authority)

NMOT CONDITIONS

Maximum power	[Pmpp]	Wp	164	IEC 61215
Voltage at maximum power	[Vmpp]	V	21,72	
Current at maximum power	[Impp]	A	7,56	
Open circuit voltage	[Voc]	V	25,76	
Short circuit current	[Isc]	A	7,98	

NMOT (Nominal Module Operating Temperature): Irradiance: 800 W/m2 + Ambient Temperature: 20º C + Air Mass: 1.5 + Wind Speed: 1 m/s

MECHANICAL CHARACTERISTICS

PANEL	WIDTH (X)		HIGH (Y)		DIAGONAL	AREA	POWER/AREA
Size - Glass-1	1000	x	1260	mm		1,26 m2	176 Wp/m2
Size - Glass-2	1000	x	1260	mm		1,26 m2	
CELLS							
Size	156,75	x	156,75	mm	210 mm	0,02 m2	
Distance - Top			31	mm			
Distance - between Cells	4	x	4	mm			
Distance - Left	20	mm					
Distance - Right	20	mm					
Distance - Bottom			109	mm			
Quantity	6	x	7	=	42 units	1,03 m2	

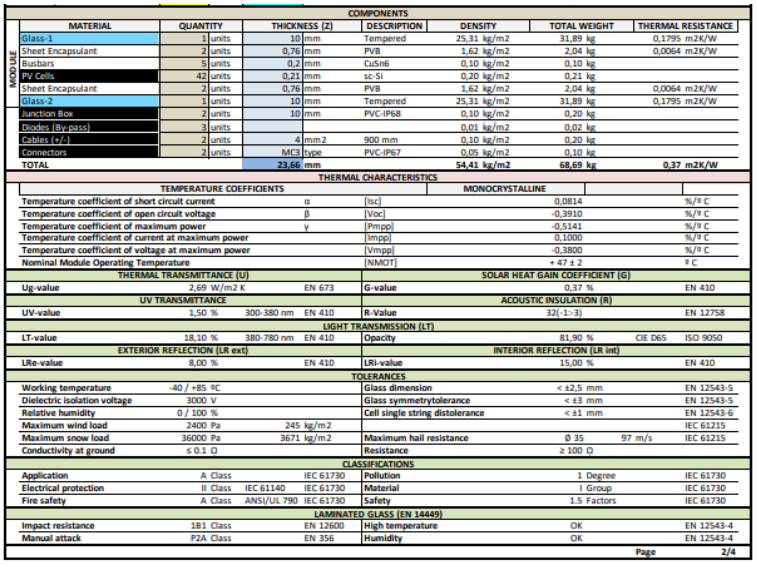

COMPONENTS

	MATERIAL	QUANTITY		THICKNESS (Z)		DESCRIPTION	DENSITY	TOTAL WEIGHT	THERMAL RESISTANCE
MODULE	Glass-1	1	units	10	mm	Tempered	25,31 kg/m2	31,89 kg	0,1795 m2K/W
	Sheet Encapsulant	2	units	0,76	mm	PVB	1,62 kg/m2	2,04 kg	0,0064 m2K/W
	Busbars	5	units	0,2	mm	Cu5n6	0,10 kg/m2	0,10 kg	
	PV Cells	42	units	0,21	mm	sc-Si	0,20 kg/m2	0,21 kg	
	Sheet Encapsulant	2	units	0,76	mm	PVB	1,62 kg/m2	2,04 kg	0,0064 m2K/W
	Glass-2	1	units	10	mm	Tempered	25,31 kg/m2	31,89 kg	0,1795 m2K/W
	Junction Box	2	units	10	mm	PVC-IP68	0,10 kg/m2	0,20 kg	
	Diodes (By-pass)	3	units				0,01 kg/m2	0,02 kg	
	Cables (+/-)	2	units	4	mm2	900 mm	0,10 kg/m2	0,20 kg	
	Connectors	2	units	MC3	type	PVC-IP67	0,05 kg/m2	0,10 kg	
	TOTAL			23,66	mm		54,41 kg/m2	68,69 kg	0,37 m2K/W

THERMAL CHARACTERISTICS

TEMPERATURE COEFFICIENTS		MONOCRYSTALLINE		
Temperature coefficient of short circuit current	α	[Isc]	0,0814	%/º C
Temperature coefficient of open circuit voltage	β	[Voc]	-0,3910	%/º C
Temperature coefficient of maximum power	γ	[Pmpp]	-0,5141	%/º C
Temperature coefficient of current at maximum power		[Impp]	0,1000	%/º C
Temperature coefficient of voltage at maximum power		[Vmpp]	-0,3800	%/º C
Nominal Module Operating Temperature		[NMOT]	+ 47 ± 2	º C

THERMAL TRANSMITTANCE (U)				SOLAR HEAT GAIN COEFFICIENT (G)		
Ug-value	2,69 W/m2 K	EN 673		G-value	0,37 %	EN 410
UV TRANSMITTANCE				**ACOUSTIC INSULATION (R)**		
UV-value	1,50 %	300-380 nm	EN 410	R-Value	32(-1;-3)	EN 12758
LIGHT TRANSMISSION (LT)						
LT-value	18,10 %	380-780 nm	EN 410	Opacity	81,90 %	CIE D65 ISO 9050
EXTERIOR REFLECTION (LR ext)				**INTERIOR REFLECTION (LR int)**		
LRe-value	8,00 %		EN 410	LRi-value	15,00 %	EN 410

TOLERANCES

Working temperature	-40 / +85 ºC		Glass dimension	< ±2,5 mm	EN 12543-5
Dielectric isolation voltage	3000 V		Glass symmetrytolerance	< ±3 mm	EN 12543-5
Relative humidity	0 / 100 %		Cell single string distolerance	< ±1 mm	EN 12543-6
Maximum wind load	2400 Pa	245 kg/m2			IEC 61215
Maximum snow load	36000 Pa	3671 kg/m2	Maximum hail resistance	Ø 35	97 m/s IEC 61215
Conductivity at ground	≤ 0.1 Ω		Resistance	≥ 100 Ω	

CLASSIFICATIONS

Application	A Class		IEC 61730	Pollution	1 Degree	IEC 61730
Electrical protection	II Class	IEC 61140	IEC 61730	Material	I Group	IEC 61730
Fire safety	A Class	ANSI/UL 790	IEC 61730	Safety	1.5 Factors	IEC 61730

LAMINATED GLASS (EN 14449)

Impact resistance	1B1 Class	EN 12600	High temperature	OK	EN 12543-4
Manual attack	P2A Class	EN 356	Humidity	OK	EN 12543-4

Page 2/4

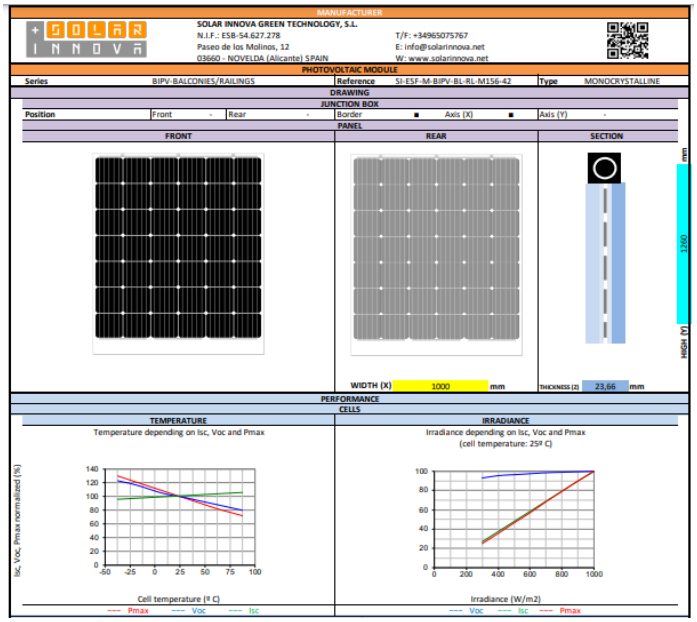
MANUFACTURER
SOLAR INNOVA GREEN TECHNOLOGY, S.L.
N.I.F.: ESB-54.627.278
Paseo de los Molinos, 12
03660 - NOVELDA (Alicante) SPAIN
T/F: +34965075767
E: info@solarinnova.net
W: www.solarinnova.net
PHOTOVOLTAIC MODULE
Series
BIPV-BALCONIES/RAILINGS
Reference
SI-ESF-M-BIPV-BL-RL-M156-42
Type
MONOCRYSTALLINE
DRAWING
JUNCTION BOX
Position
Front
Rear
Border
Axis (X)
Axis (Y)
PANEL
FRONT
REAR
SECTION
WIDTH (X)
1000
mm
THICKNESS (Z)
23,66
mm
PERFORMANCE
CELLS
TEMPERATURE
Temperature depending on Isc, Voc and Pmax
Isc, Voc, Pmax normalized (%)
Cell temperature (º C)
Pmax
Voc
Isc
IRRADIANCE
Irradiance depending on Isc, Voc and Pmax
(cell temperature: 25º C)
Irradiance (W/m2)
Voc
Isc
Pmax

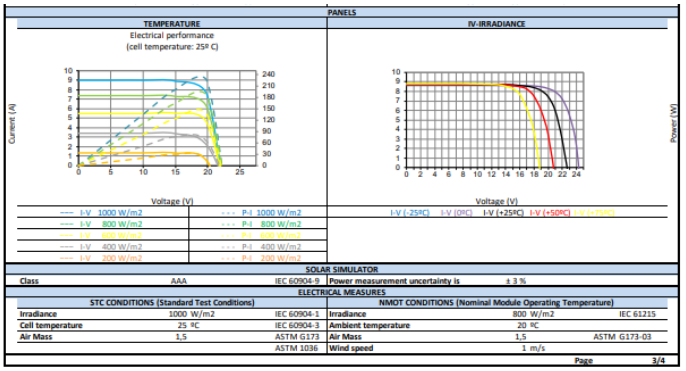
PANELS
TEMPERATURE
Electrical performance
(cell temperature: 25º C)
Current (A)
Voltage (V)
I-V 1000 W/m2
P-I 1000 W/m2
I-V 800 W/m2
P-I 800 W/m2
I-V 600 W/m2
P-I 600 W/m2
I-V 400 W/m2
P-I 400 W/m2
I-V 200 W/m2
P-I 200 W/m2
IV-IRRADIANCE
Power (W)
Voltage (V)
I-V (-25ºC)
I-V (0ºC)
I-V (+25ºC)
I-V (+50ºC)
SOLAR SIMULATOR
Class
AAA
IEC 60904-9
Power measurement uncertainty is
± 3 %
ELECTRICAL MEASURES
STC CONDITIONS (Standard Test Conditions)
Irradiance
1000 W/m2
IEC 60904-1
Cell temperature
25 ºC
IEC 60904-3
Air Mass
1,5
ASTM G173
ASTM 1036
NMOT CONDITIONS (Nominal Module Operating Temperature)
Irradiance
800 W/m2
IEC 61215
Ambient temperature
20 ºC
Air Mass
1,5
ASTM G173-03
Wind speed
1 m/s
Page
3/4

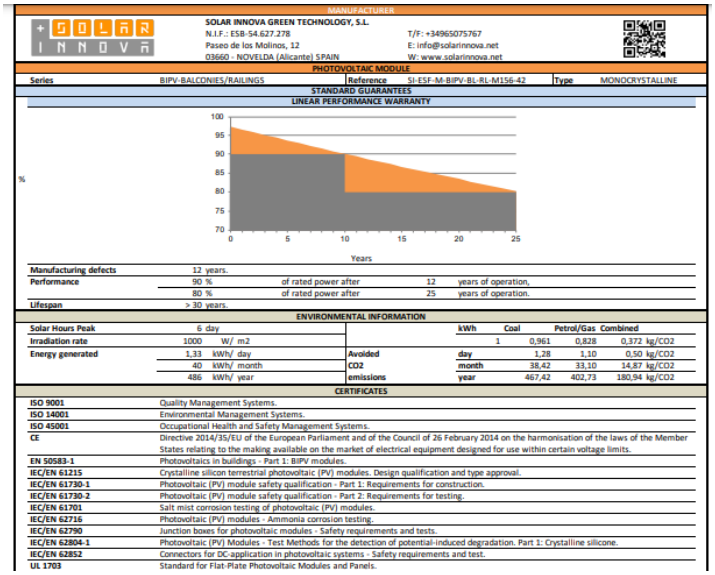
MANUFACTURER
SOLAR INNOVA GREEN TECHNOLOGY, S.L.
N.I.F.: ESB-54.627.278
Paseo de los Molinos, 12
03660 - NOVELDA (Alicante) SPAIN
T/F: +34965075767
E: info@solarinnova.net
W: www.solarinnova.net
PHOTOVOLTAIC MODULE
Series
BIPV-BALCONIES/RAILINGS
Reference
SI-ESF-M-BIPV-BL-RL-M156-42
Type
MONOCRYSTALLINE
STANDARD GUARANTEES
LINEAR PERFORMANCE WARRANTY
%
Years
Manufacturing defects
12 years.
Performance
90 % of rated power after 12 years of operation,
80 % of rated power after 25 years of operation.
Lifespan
> 30 years.
ENVIRONMENTAL INFORMATION
Solar Hours Peak
6 day
Irradiation rate
1000 W/ m2
Energy generated
1,33 kWh/ day
40 kWh/ month
486 kWh/ year
kWh
Coal
Petrol/Gas
Combined
1
0,961
0,828
0,372 kg/CO2
Avoided CO2 emissions
day
1,28
1,10
0,50 kg/CO2
month
38,42
33,10
14,87 kg/CO2
year
467,42
402,73
180,94 kg/CO2
CERTIFICATES
ISO 9001
Quality Management Systems.
ISO 14001
Environmental Management Systems.
ISO 45001
Occupational Health and Safety Management Systems.
CE
Directive 2014/35/EU of the European Parliament and of the Council of 26 February 2014 on the harmonisation of the laws of the Member States relating to the making available on the market of electrical equipment designed for use within certain voltage limits.
EN 50583-1
Photovoltaics in buildings - Part 1: BIPV modules.
IEC/EN 61215
Crystalline silicon terrestrial photovoltaic (PV) modules. Design qualification and type approval.
IEC/EN 61730-1
Photovoltaic (PV) module safety qualification - Part 1: Requirements for construction.
IEC/EN 61730-2
Photovoltaic (PV) module safety qualification - Part 2: Requirements for testing.
IEC/EN 61701
Salt mist corrosion testing of photovoltaic (PV) modules.
IEC/EN 62716
Photovoltaic (PV) modules - Ammonia corrosion testing.
IEC/EN 62790
Junction boxes for photovoltaic modules - Safety requirements and tests.
IEC/EN 62804-1
Photovoltaic (PV) Modules - Test Methods for the detection of potential-induced degradation. Part 1: Crystalline silicone.
IEC/EN 62852
Connectors for DC-application in photovoltaic systems - Safety requirements and test.
UL 1703
Standard for Flat-Plate Photovoltaic Modules and Panels.

Inverter: Solax X3-MIC-8K-G2

X3-MIC G2 (THREE PHASE)

	X3-MIC-3K-G2	X3-MIC-4K-G2	X3-MIC-5K-G2	X3-MIC-6K-G2	X3-MIC-8K-G2	X3-MIC-10K-G2	X3-MIC-12K-G2	X3-MIC-15K-G2
DC INPUT								
Max. PV array input power [Wp]	6000	8000	10000	12000	16000	20000	24000	30000
Max. PV input voltage [V]	1000	1000	1000	1000	1000	1000	1000	1000
Startup voltage [V]	150	150	150	150	150	150	150	150
Nominal input voltage [V]	640	640	640	640	640	640	640	640
MPP tracker voltage range [V]	120~980	120~980	120~980	120~980	120~980	120~980	120~980	120~980
No. of MPP trackers/Strings per MPP tracker	2(1/1)	2(1/1)	2(1/1)	2(1/1)	2(1/1)	2(1/1)[1]	2(2/1)	2(2/1)
Max. input current[A]	16/16	16/16	16/16	16/16	16/16	16/16[1]	32/16	32/16
Max. short circuit current[A]	20/20	20/20	20/20	20/20	20/20	20/20[1]	40/20	40/20
AC OUTPUT								
Nominal AC output power [W]	3000	4000	5000	6000	8000	10000	12000	15000
Nominal AC output current [A]	4.6/4.4	6.1/5.8	7.6/7.3	9.1/8.7	12.2/11.6	15.2/14.5	18.2/17.4	22.7/21.8
Max. AC output apparent power [VA]	3300	4400	5500	6600	8800	11000	13200	15000
Max. AC output current [A]	4.8	6.4	8.0	9.6	12.8	16.0	19.1	22.7
Nominal AC voltage [V]	220/380V, 230/400V, 3/N/PE							
Nominal grid frequency/Grid frequency [Hz]	50/60							
Displacement power factor	0.8 leading-0.8 lagging							
THDi (Rated power) [%]	<3							

SYSTEM DATA								
Max. efficiency [%]	98.3	98.3	98.3	98.3	98.3	98.3	98.3	98.3
Euro efficiency [%]	97.8	97.8	97.8	97.8	97.8	97.8	97.8	97.8
Standby consumption (night) [W]	<3							
Ingress protection	IP66							
Operating temperature range [°C]	-30~+60(Derating above 45)							
Max. operation altitude [m]	4000(Derating above 3000)							
Relative humidity [%]	0~100							
Typical noise emission [dB]	<30	<30	<30	<30	<45	<45	<50	<50
Storage temperature [°C]	-30~+60							
Dimensions (WxHxD) [mm]	342*434*144.5				342*434*156			
Weight [kg]	15.5	15.5	15.5	15.5	17	17	18	18
Cooling concept	Natural cooling				Smart fan cooling			
Communication interfaces	USB / RS485 / DRM / Pocket WiFi (Optional: Pocket LAN/4G) / Adapter box(Optional)							
PROTECTION								
Over/under voltage protection	YES							
DC isolation protection	YES							
DC reverse protection	YES							
Grid monitoring	YES							
DC injection monitoring	YES							
Back feed current monitoring	YES							
Residual current detection	YES							
Anti-islanding protection	YES							
Over temperature protection	YES							
SPD (DC/AC)	Type III / Type III							
Arc-fault circuit interrupter(AFCI)	Optional							
AC auxiliary power supply(APS)	Optional							
STANDARD								
Safety	IEC/EN 62109-1; IEC/EN 62109-2; NB/T 32004							
EMC	IEC/EN 61000; NB/T 32004							
Cetification	VDE4105; EN 50549; AS 4777.2; VDE4105; IEC 61727; IEC 62116; IEC 61683; IEC 60068; EN 50530; NB/T 32004							

A2. Economic Summary

The economic summary presents the costs and equipment prices associated with the study and consolidated detailed information obtained through market research and cost analysis.

Equipment	Cost/Unit (Euros)	Number of units	Total cost (Euros)	Supplier
High Roof				
Jinko Solar 580 bifacial	164	54	8,856	LM8 Solar, Spain
Huawei- SUN2000-30KTL-M3	2,900	1	2,900	Efecto Solar, Spain
Installation cost (20% of equipment price)			2,351.2	
Yearly Maintenance (1.5% of equipment price)			176.34	
Facade 1-A				
Jinko Solar 585	144	52	7,488	LM8 Solar, Spain
Solax X3-PRO G2-25	2,800	1	2,800	LM8 Solar, Spain
Installation cost (20% of equipment price)			2,057.6	
Yearly Maintenance (1.5% of equipment price)			154.32	
Facade 1-B				
Jinko Solar 585	144	153	22032	LM8 Solar, Spain
Huawei- SUN2000-36KTL-M3	3,300	2	6,600	LM8 Solar, Spain
Installation cost (20% of equipment price)			5,726.4	
Yearly Maintenance (1.5% of equipment price)			429.48	
Facade 2				
Jinko Solar 630	155	114	17,670	LM8 Solar, Spain
Huawei- SUN2000-60KTL-M3	3,650	1	3,650	LM8 Solar, Spain
Installation cost (20% of equipment price)			4,264	
Yearly Maintenance (1.5% of equipment price)			319.8	

Balcony Terrasse				
SolarInnova-222 Wp	550	42	23,100	Solar Innova, Spain
Solax X3-MIC G2 -8k	1,600	1	1,600	LM8 Solar, Spain
Support bar	600	7	4,200	Solar Innova, Spain
Installation cost (20% of equipment price)			5,780	
Yearly Maintenance (1.5% of equipment price)			433.5	
Total Cost			**121,075.2**	
Total Maintenance Cost (Yearly)			**1,513.44**	